STRUCTURAL, MAGNETIC AND TRANSPORT PROPERTIES OF SPINEL TYPE $Li_{0.5-x/2}Cu_xFe_{2.5-x/2}O_4$

M. Phil Thesis

SUBMITTED BY

MUHAMMAD SAMIR ULLAH

ROLL NO. : 100614036P

SESSION : October - 2006

A THESIS SUBMITTED TO THE DEPARTMENT OF PHYSICS, BANGLADESH UNIVERSITY OF ENGINEERING & TECHNOLOGY, DHAKA, IN PARTIAL FULFILLMENT OF THE REQUIREMENT FOR THE DEGREE OF MASTER OF PHILOSOPHY IN PHYSICS

DEPARTMENT OF PHYSICS

BANGLADESH UNIVERSITY OF ENGINEERING & TECHNOLOGY

DHAKA-1000, BANGLADESH

BANGLADESH UNIVERSITY OF ENGINEERING AND TECHNOLOGY
DEPARTMENT OF PHYSICS, DHAKA-1000

Certification of thesis work

The thesis titled **"STRUCTURAL, MAGNETIC AND TRANSPORT PROPERTIES OF SPINEL TYPE $Li_{0.5-x/2}Cu_xFe_{2.5-x/2}O_4$"**, submitted by **MUHAMMAD SAMIR ULLAH**, Roll No.: 100614036P, Session: October/2006, has been accepted as satisfactory in partial fulfillment of the requirement for the degree of **Master of Philosophy (M. Phil.) in Physics** on 20 October, 2010.

BOARD OF EXAMINERS

1. _____
DR. MD. FEROZ ALAM KHAN (Supervisor) — Chairman
Professor
Department of Physics
BUET, Dhaka-1000

2. _____
DR. SHEIKH MANJURA HOQUE (Co-Supervisor) — Member
Principal Scientific Officer
Materials Science Division
AECD, Dhaka-1000

3 A. Hossain
DR. A. K. M. AKTHER HOSSAIN — Member
Professor and Head
Department of Physics
BUET, Dhaka-1000

4. Jiban Podder
DR. JIBAN PODDER — Member
Professor
Department of Physics
BUET, Dhaka-1000

5. _____
DR. MAQBULUR RAHMAN — Member (External)
Professor
Department Physics
University of Dhaka, Dhaka-1000

Candidate's Declaration

It is hereby declared that this thesis or any part of it has not been submitted elsewhere for the award of any degree or diploma.

MUHAMMAD SAMIR ULLAH

Dedicated to

My Parents

&

Daughter

Acknowledgements

All the admiration to the almighty Allah, the most merciful and beneficial, has enabled me to do this thesis work leading to the M.Phil. degree.

It is a great pleasure to express my deepest sense of gratitude and sincere appreciation to my reverend supervisor, Prof. Dr. Md. Feroz Alam Khan, Department of Physics, Bangladesh University of Engineering and Technology (BUET), Dhaka-1000, for his scholastic supervision, erudite discussion and constructive guidance through out the progress of this research work.

I would like to express my deepest sense of gratitude and thanks to my co-supervisor Dr. Sheikh Manjura Hoque, Principal Scientific Officer, Materials Science Division, Atomic Energy Center, Dhaka-1000, for her kind cooperation and constructive guidance during my research work.

I am very greatful to Prof. Dr. A. K. M. Akther Hossain, Head, Department of Physics, Bangladesh University of Engineering and Technology (BUET), Dhaka-1000 for his cooperation during my research work.

I am very greatful to the Dr. A. K. M. Abdul Hakim, Head, Materials Science Division, Atomic Energy Center, Dhaka-1000, for his cooperation during my research work.

I heartily express my gratitude to Prof. Dr. Mominul Huq, Prof. Dr. Md. Abu Hashan Bhuiyan, Prof. Dr. Nazma Zaman, Prof. Dr. Jiban Podder, Prof. Dr. Md. Mostak Hossain and Dr. D. K. Saha for their cooperation during my research work.

I would like to express my coordial thanks to Dr. Nazrul Islam, Mrs. Fahima Khanam, Dr. Afia Begum, Dr. Md. Rafi Uddin, Dr. Md. Forhad Mina, Dr. Nasreen Akter, Muhammad Rakibul Islam, Mohammad Jellur Rahman, Mohammad Abu Sayem Karal, Muhammad Ruhul Amin, Mohammad Khorshed Alam, Roma Bijoy Sarker, Sunirmol Majumdar, Ferdousi Apa and Md. Kamruzzaman for their important suggestions during my research work.

I would mention a very special thanks for the moral support and inspiration provided by the my wife Nasrin Parvin during my research work.

ABSTRACT

$Li_{0.5-x/2}Cu_xFe_{2.5-x/2}O_4$ ferrites were sintered at three different temperatures 1200, 1100 and 1000^oC, in air for 3 hours, where x in the range of 0.0 to1.0. Samples were also sintered at 800^oC for x = 0.9 and 1.0. Samples were prepared by solid state reaction technique. X-ray diffraction technique was used to study the structure of above mentioned ferrites in the range of $0.0 \leq x \leq 1.0$. For the sintering temperature of 1000^oC, $Li_{0.5-x/2}Cu_xFe_{2.5-x/2}O_4$ undergoes cubic to tetragonal transformation for higher Cu content. However, this tetragonal deformation could not be observed for the sintering temperatures of 1100 and 1200^oC in the x-ray diffraction pattern. Composition dependence of lattice parameter has been observed and it does not follow the Vegard's law in higher Cu content because of structural change at higher Cu content for higher sintering temperature. The saturation magnetization has been measured by a home built Vibrating Sample Magnetometer (VSM) at room temperature. The measurement shows that the saturation magnetization decreases with the increase of Cu content. This is due to the fact that the decrease of A-B interaction is observed to be weakened with increasing of Cu^{2+} ions. Using the values of saturation magnetization, the experimental magnetic moment (Bohr magneton) has been calculated for different samples. The thermal variation of the initial permeability μ_i was measured to determine the Curie temperature T_C, for the toroid shape samples. Curie temperatures of $Li_{0.5-x/2}Cu_xFe_{2.5-x/2}O_4$ ferrites were found to decrease with the increase of Cu^{2+} content due to the reduction of A-B interaction. Curie temperature reduces linearly up to x = 0.5 for sintering temperature of 1100^oC and x = 0.7 for sintering temperature of 1200^oC, respectively, and nonlinearity at higher Cu content decreases with the increase of sintering temperature. The real part of the complex initial permeability μ_i for frequency up to f = 13 MHz have been measured. It is observed that the initial permeability is higher for higher Cu content. The B-H loops were measured for the $Li_{0.5-x/2}Cu_xFe_{2.5-x/2}O_4$ ferrites at constant frequency f = 1200 Hz at room temperature. Coercivity and hysteresis loss are decreased with the increase of Cu content due to increased of magnetic softness at the Cu-rich end. The transport property, in particular, electrical resistivity has been investigated as function of temperature. It is observed that ferrites are of semiconductor nature and their resistivity decreases with increasing of temperatures. At room temperature, the resistivity increases up to x = 0.3, but it

decreases for x > 0.3, which can be attributed to the decrease of Fe^{3+} and Li^{+} concentration with increase of Cu content, but Fe^{2+} ions are increased. This indicates that Fe^{+2} ions are present as traces in the samples of x > 0.3. Activation energy has been calculated for different compositions and it is increased with increase of Cu content. The thermal variation of dielectric constant was measured for different composition. It is observed that the dielectric constant increases slowly in the beginning and after that dielectric constant increases rapidly for different samples. As the temperature is increased, thermal energy provided to the sample plays a role to decrease the relaxation time and hence there is an increase in dielectric constant. Dielectric constant has been observed as a function of frequency and it decreases with increase of frequency.

LIST OF FIGURES

Chapter-2

Chapter-4

Chapter-5

LIST OF TABLES

Pages

CONTENTS

CHAPTER ONE

General Introduction

1.1 Introduction

Soft ferrites have been extensively used for different kinds of magnetic devices such as transformers, inductors and magnetic heads for high frequency applications because of their electrical resistivity is higher than those of the soft magnetic alloys [1] Ferrites are important component for electrical, electronic, telecommunication and data storage system. Exhaustive research is very much necessary to develop the application of ferrites in electrical and electronic industries. These applications oriented materials are also important for the research on which provides potential opportunity to consolidate the knowledge of fundamental research on ferrimagnetisms and condensed matter physics.

Ferrimagnetic substances, often referred to as *ferrites*, are certain double oxides of iron and another metal whose chemical composition is of the form $XO.Fe_2O_3$ or XFe_2O_4, where X signifies a divalent metal [2]. These often crystallize in the *spinel* structure. Spinel ferrites have two sublattices, tetrahedral (or A site) and octahedral (or B site) in AB_2O_4 crystal structure. The cation arrangement can vary into two cases: one is the normal spinel, where all divalent cations are occupy in A site and all the trivalent cations are occupy in B site. The other is the inverse spinel, where all the divalent ions are occupy in B site, and the trivalent cations equally divided into both A and B sites. Spinel with cation distribution intermediate between these two extreme cases, known as mixed spinel.

Spinel ferrites are compounds of iron oxides and some transition metal oxides and they exhibit certain important electrical and magnetic properties, which make them extensively used in technological and industrial applications as magnetic storage and in microwave devices Among them, Li-ferrites emerged as a good microwave device material due to their high Curie temperature, high squareness ratio, superior temperature stability of saturation magnetization and low magnetic losses [3]. Many factors such as processing conditions, type and amount of doped impurities affect the quality and hence the performance of these materials. Modifications in the properties of the lithium ferrite $Li_{0.5}Fe_{2.5}O_4$ due to the substitution of various ions have been studied by several workers. Various studies can be found in the literature on Li-Ti, Li-Ge, Li-Cd and Li-Zn ferrites [4-5]. There are scanty of data on Li-Cu

system in the literature. Few investigators have focused their attention on Cu substituted mixed spinel ferrite because Cu containing have interesting magnetic and electrical properties. Copper ferrite, $CuFe_2O_4$ is distinguished among other spinel ferrites by the fact that it undergoes a structural phase transition accompanied by a reduction in the crystal symmetry to tetragonal due to the cooperative Jahn-Teller effect [6]. Most of these ferrites are in non-cubic structure at low temperatures and spinel at high temperatures. $CuFe_2O_4$ is distorted inverse spinels and its distortion can be explained by Jahn-Teller effect Cu^{2+} is a d^9 cation and orbitals are occupied by unpaired electrons. Therefore, it is interesting to Cu^{2+}substituted Li-ferrite to understand the structural and magnetic properties. There have been many investigations of magnetic spectra of various ferrites in a wide range of frequencies. The initial permeability of ferromagnetic materials results from the spin rotational and domain wall motion. Useful frequency range of ferrite is limited by the onset of resonance phenomenon for which either the permeability begins to fall at a critical frequency or the losses rise sharply. Hence the knowledge of the frequency dependence of initial permeability and losses are necessary.

In this research, $Li_{0.5-x/2}Cu_xFe_{2.5-x/2}O_4$ where x = 0 to 1, samples are sintered at 1000, 1100 and 1200^{o}C. Formation of single phase ferrite was confirmed by X-ray diffractometer (XRD). Crystal structure, lattice parameter and X-ray density were determined from XRD data. The variations of X-ray and bulk densities were observed as a function of Cu content of the samples. It is clearly shown that both densities increase with increasing of Cu content. This can be ascribed to the atomic weight and density of Cu^{2+} (63.55 amu, 8.96 g/cm^3, respectively) which are higher than that of Li^+ (6.94 amu, 0.53 g/cm^3) and Fe^{3+} (55.85 amu, 7.87 g/cm^3) [7]. Therefore, the porosity of the investigated samples was calculated as a function of Cu content. In this case, porosity of the sample decreases with increase of Cu content. Magnetization is defined as the magnetic moment per unit volume. There are various techniques of measuring magnetization of a substance. In the present thesis saturation magnetization has been measured by a home built vibrating sample magnetometer (VSM) at room temperature. It can be seen that the saturation magnetization decreases with increase of Cu^{2+} ion concentration due to the average A-B interaction gets smaller. Curie temperature, T_C is a measure of exchange force in ferrimagnetisms. At this temperature, ferrimagnetic

substance thus changes to a paramagnetic substance. T_C decreases with increasing of Cu content. This behavior can be explained as follows: the substitution of the high spin quantum number ion Fe^{3+} by the low spin quantum number ion Cu^{2+} either at B-site or A-site, weakens the A-B interaction. This leads to a decreases to saturation magnetization and consequently Curie temperature, T_C. Polycrystalline ferrites having very high dielectric constants that are used in good microwave devices such as isolators, circulators. Dielectric properties of ferrites are dependent on the method of preparation and substitution of different ions The ferrites behave as inhomogeneous dielectric materials in which individual high conducting grains are separated by either air gaps or low conducting layers. As a consequence of the inhomogeneous dielectric behaviour, dielectric constant as high as 10^5 are found at low frequencies in ferrites.[[8-9]. Li ferrites which have important materials for microwave applications because of their low costs and low dielectric losses.

1.2 Objective of the Present Work

$Li_{0.5}Fe_{2.5}O_4$ has highest magnetic moment of all ferrites. Numerous data can be found on Li-ferrite substituted by other elements. There has been less studies on Li-Cu ferrite system though Cu containing ferrite exhibit interesting structural, magnetic and electrical properties. Therefore, it is interesting to substitution of Cu with Li to understand its effect on the structural, magnetic and electrical properties.

The aim of the present research are

i) Preparation of various $Li_{0.5-x/2}Cu_xFe_{2.5-x/2}O_4$ samples in the range of $0 \bullet x \bullet 1$ by standard double sintering ceramic method.

ii) Determination of lattice parameter, x-ray and bulk densities and porosity of the samples.

iii) Study of the microstructure of $Li_{0.5-x/2}Cu_xFe_{2.5-x/2}O_4$ by Scanning Electron Microscope (SEM) and evaluation of average grain size with the help of linear intercept technique.

iv) Measurement of saturation magnetization at room temperature by a home built VSM and evaluation of experimental Bohr magneton for different compositions.

v) Determination of ferrimagnetic to paramagnetic transition temperature, T_c from the measurement of the temperature dependence of initial permeability.

vi) Evaluation of initial permeability as a function of frequency (1kHz -13MHz) for samples of $0 \bullet x \bullet 1$.

vii) Study of B-H loops by BH Loop Tracer and evaluation of coercivity and hysteresis loss.

viii) Study of the temperature dependence of electrical resistivity and dielectric constant and determination of the activation energy for different compositions.

ix) Study of the dielectric constant in the frequency range 10 kHz to 500 kHz.

1.3 Organization of this Thesis Paper

The organization of the thesis is as follows:

Chapter-1 of the thesis deals with a brief overview of materials, importance and objectives of the present work.

Chapter–2 gives the theoretical background and the crystal structure of the spinel ferrites.

Chapter- 3 gives the details of the sample preparation.

Chapter-4 describes the experimental part and descriptions of different measurement techniques that have been used in this research work.

Chapter-5 is devoted to the results of various investigations of the study and their interpretation based on the existing theories and models.

The conclusions drawn from the overall experimental results and discussion are presented in **Chapter -6**

References:

[1]S. Manjura. Hoque, Md. Amanullah Choudhury, Md. Fakrul. Islam, "*Characterization of Ni-Cu Mixed Spinel Ferrite*" J. Magn. Magn. Mater. 251, 292, (2002)

[2] M. Ali Omar, *Elementary Solid State Physics,* Addison-Wesley, p.453, (2000)

[3] M. Maisnam, S. Phanjoubam, H. N. K. Sarma, O. P. Thakur, L. Radhapiyari Devi and Chandra Prakash, "Influence of temperature on the dielectric behaviour of Co^{2+} substituted Li-Ni-Mn ferrites" Ind. J. Engg. Mat. Sci. 15, 199, (2008)

[4] S. A. Mazen, M. H. Abdullah, R. I. Nakhla, F. Metawe, H. M. Zaki, "*X-ray analysis and IR absorption spectra of Li-Ge ferrite*" Mater. Chem. Phys 34, 35, (1993)

[5] A. A. Yousif, E. Elazain, S. A. Mazen, H. H Sutherland, M. H. Abdullah, S. F. Mansour, "*A Mossbauer and X-ray diffraction investigation of Li-Ti ferrites*" J. Phys. Condensed Matter. 6, 5717, (1994)

[6] J. D. Dunitz, L.E. Orgel, "*Electronic properties of transition metal oxides: Part I, Distortions from cubic symmetry"* J. Phys. Chem. Solids, 3, 20, (1957)

[7] William D. Callister, An Introduction Materials Science and Engineering, John Wiley & Sons, Inc. (2001)

[8] S. A. Mazen, "*Infrared absorption and dielectric properties of Li-Cu ferrite*", Mat.Chem.Phys. 62, 139, (2000)

[9] A. M. Shaikh, S. S. Bellad, B. K. Chougule, " *Temperature and frequency dependent dielectric properties of Zn substituted Li-Mg ferrites"* J. Magn. Magn. Mater. 195, 384, (1999)

CHAPTER TWO

General Features of Spinel Oxides

2.1 Spinel Oxides

Ferrites have the cubic structure, which is very close to mineral spinel $MgO.Al_2O_3$ and are called cubic spinels. Analogous to the mineral spinel, magnetic spinel have the general formula, $MeO.Fe_2O_3$ or $MeFe_2O_4$, where *Me* is the divalent metal ion [1]. The structure was first determined by Bragg [2] and Nishikawa [3]. Formerly, spinels containing *Fe* were called ferrites, but now the term has been broadened to include many other ferrimagnets including garnets and hexagonal ferrites and these need not necessarily contain iron. In the ideal spinel structure the anions form cubic close packing, in which the cations partly occupy the tetrahedral (A-sites) and octahedral (B-sites) interstices. Now, the interstices are not all the same: some which we call A-sites are surrounded by or coordinated with 4 nearest neighboring oxygen ions whose lines connecting their centers form a tetrahedron. Thus, A-sites are called tetrahedral sites. The other types of B-sites are coordinated by 6 nearest neighboring oxygen ions whose lines connecting their centers form an octahedron. Thus B-sites are called octahedral sites. In the unit cell of 32 oxygen ions there are 64 tetrahedral sites and 32 octahedral sites. It turns out that of the 64 tetrahedral sites, only 8 are occupied and out of 32 octahedral sites, only 16 are occupied. Thus structure of spinel compounds is complex; the unit cell contains 8 formula units AB_2O_4, with 8 A-sites, 16 B-sites and 32 oxygen ions, and total of 8×7 = 56 ions. A spinel unit cell contains two types of sub cells, the two types of sub cells alternate in a three dimensional array so that each fully repeating unit cell requires 8 sub cells. The positions of the ions in the spinel lattice are not perfectly regular and some distortion does occur .The tetrahedral sites are often too small for the metal ions so that the oxygen ions move slightly to accommodate them. The oxygen ions connected with the octahedral sites move in such a way as to shrink the size the octahedral cell by the same amount as the tetrahedral site expands. The movement of the tetrahedral oxygen is reflected in a quantity called the oxygen parameter, which is the distance between the oxygen ion and the face of the cube edge along the cube diagonal of the spinel subcell. This distance is theoretically equal to $3/8a_o$ where a_o is the lattice constant.

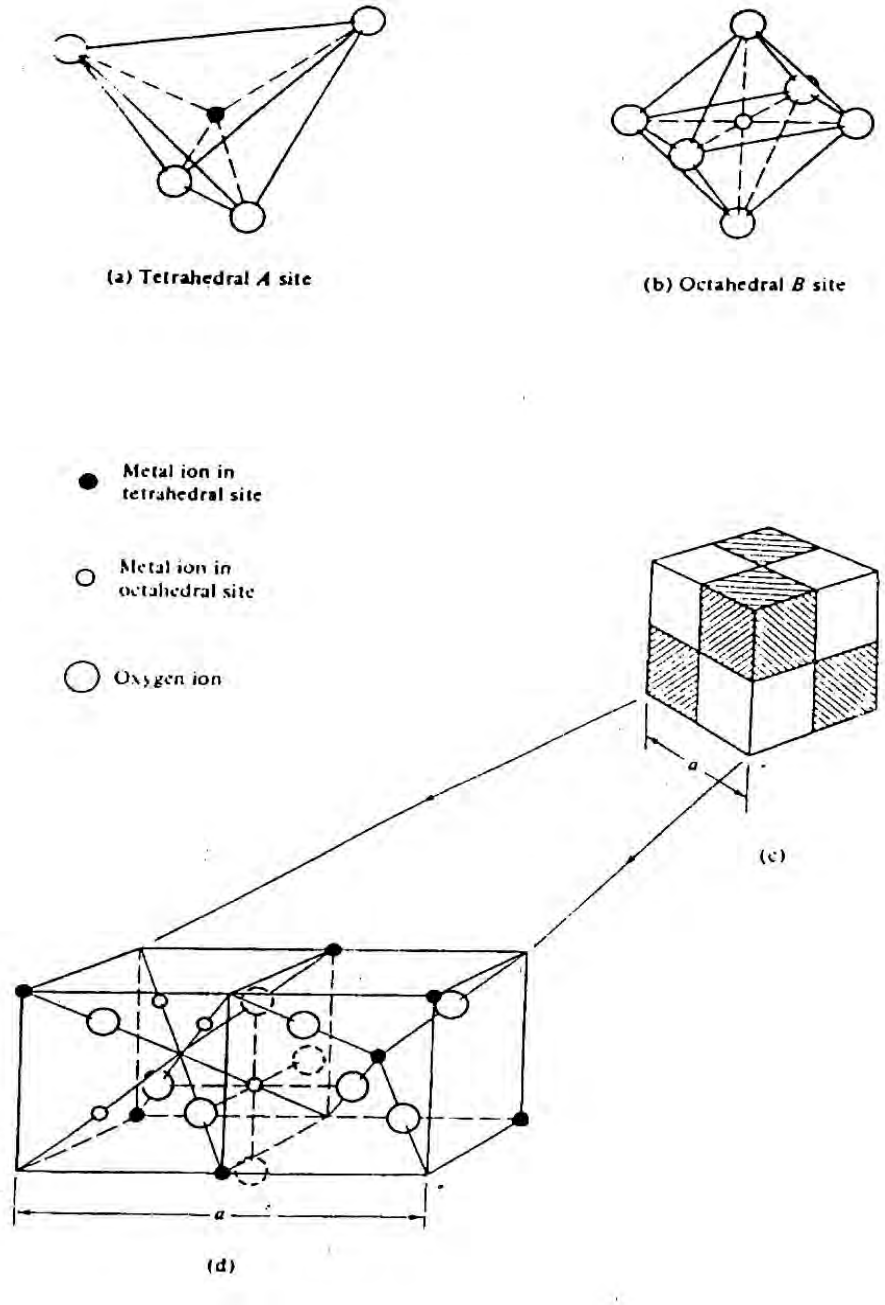

Fig. 2.1. Crystal Structure of Spinel Cubic

2.2 Cation Distribution of Spinel Ferrites

In spinel structure the distribution of cations over the tetrahedral or *A* sites and octahedral or *B* sites can be present in a variety of ways. If all the Me^{2+} ions in $Me^{2+}\ Me_2{}^{3+}O_4$ are in tetrahedral and all Me^{3+} ions in octahedral positions, the spinel is then called normal spinel. Another cation distribution in spinel exists, where one half of the cations Me^{3+} are in the A-sites and the rest, together with the Me^{2+} ions are randomly distributed among the B-sites. The spinel having the latter kind of cation distribution is known as inverse spinel. The distribution of these spinels can be summarized as [4-6]

1) Normal Spinels, i.e. the divalent metal ions are on A sites: $Me^{2+}\ [Me_2{}^{3+}]O_4$,
2) Inverse Spinels, i.e. the divalent metal ions are on B sites: $Me^{3+}\ [Me^{2+}Me_2{}^{3+}]O_4$,

A completely normal or inverse spinel represents the extreme cases, Zn ferrites have normal spinel structure and its formula may be written as $Zn^{2+}[Fe^{3+}Fe^{3+}]O_4{}^{2-}$. On the other hand, Cu ferrites have inverse spinel structure and its formula may be written as $Fe^{3+}[Cu^{2+}Fe^{3+}]O_4{}^{2-}$. There are many spinel oxides which have cation distributions intermediate between these two extreme cases and are called mixed spinels. The general cation distribution for the spinel can be indicated as:

$$(Me_x{}^{2+}\ Me_{1-x}{}^{3+})[Me_{1-x}{}^{2+}Me_{1+x}{}^{3+}]\ O_4{}^{2-}$$

where the first and third brackets represent the A and B sites respectively. For normal spinel x = 1 and inverse spinel x = 0. The quantity x is a measure of the degree of inversion. In the case of some spinel oxides x depends upon the method of preparation.

2.3 Introduction to Magnetic ordering:

The onset of magnetic order in solids has two basic requirements:

a) Individual atoms should have magnetic moments (spins)
b) Exchange interactions should exist that couple them together.

Magnetic moments originate in solids as a consequence of overlapping of the electronic wave functions with those of neighbouring atoms. This condition is best fulfilled by some transition metals and rare-earths. The exchange interactions depend sensitively upon the interatomic distance and the nature of the chemical bonds, particularly of nearest neighbour atoms. When

the positive exchange dominates, which corresponds to parallel coupling of neighbouring atomic moments (spins), the magnetic system becomes ferromagnetic below a certain temperature T_c called the Curie temperature. The common spin directions are determined by the minimum of magneto-crystalline anisotropy energy of the crystal. Therefore, ferromagnetic substances are characterized by spontaneous magnetization. But a ferromagnetic material in the demagnetized state displays no net magnetization in zero field because in the demagnetized state a ferromagnetic of macroscopic size is divided into a number of small regions called domains, spontaneously magnetized to saturation value and the directions of these spontaneous magnetization of the various domains are such that the net magnetization of the specimen is zero. The existence of domains is a consequence of energy minimization. The size and formation of these domains is in a complicated manner dependent on the shape of the specimen as well as its magnetic and thermal history. When negative exchange dominates, adjacent atomic moments (spins) align anti-parallel to each other, and the substance is said to be anti-ferromagnetic below a characteristic temperature, T_N, called the Neel temperature. In the simplest case, the lattice of an antiferromagnet is divided into two sub lattices with the magnetic moments of these in anti-parallel alignment. This results is zero net magnetization. A special case of anti-ferromagnetism is ferrimagnetism. In ferrimagnetism there are also two sub-lattices with magnetic moments in opposite directions, but the magnetization of the sub-lattices are of unequal strength resulting in a non-zero magnetization and therefore has net spontaneous magnetization. At the macroscopic level of domain structures, ferromagnetic and ferrimagnetic materials are therefore similar. The Curie and Neel temperatures characterize a phase transition between the magnetically ordered and disordered (paramagnetic) states. From these simple cases of magnetic ordering, various types of magnetic order exist, particularly in metallic substances. Because of long- range order and oscillatory nature of the exchange interaction, mediated by the conduction electrons, structures like helical, conical and modulated patterns might occur. A useful property for characterizing the magnetic materials is the magnetic susceptibility, defined as the magnetization, M, divided by the applied magnetic field, H i.e. $\chi = M/H$. The temperature dependence of susceptibility or, more accurately, inverse of susceptibility is a good characterization parameter for magnetic materials, Fig. 2.2. Fig. 2.2(e) shows that in the paramagnetic region, the variation of the inverse susceptibility with

temperature of a ferrite material is decidedly non-linear. Thus the ferrite materials do not obey the Curie-Weiss law, • = $C/(T-T_C)$

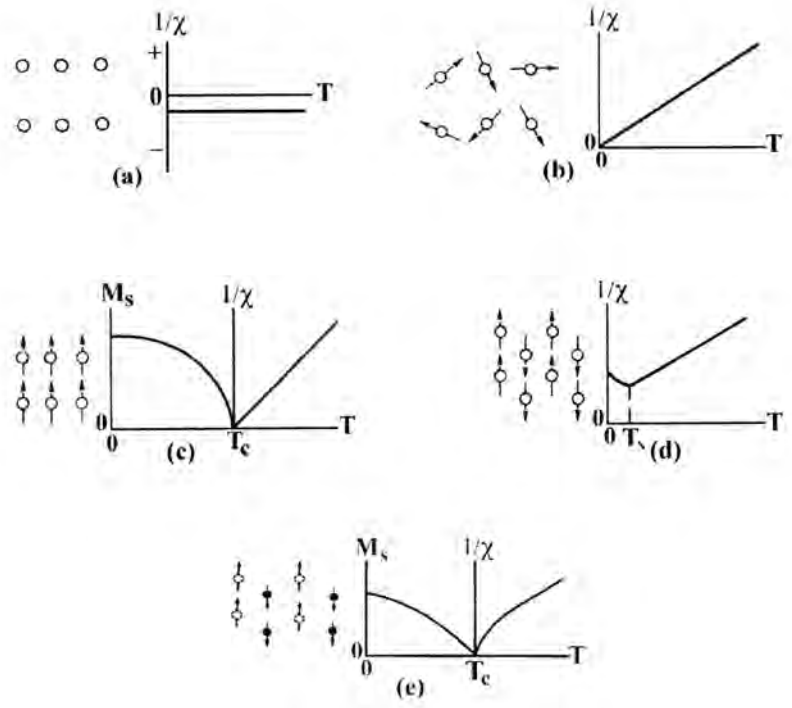

Fig.2.2. Temperature dependence of the inverse susceptibility for:(a) a diamagnetic material; (b) a paramagnetic material, showing Curie's law behavior; (c) a ferromagnetic material, showing a spontaneous magnetization for $T<T_C$ and Curie – Weiss behavior for $T>T_C$ (d) and antiferromagnetic material; (e) a ferrimagnetic material , showing a net spontaneous magnetization for $T<T_C$ and non linear behaviour for $T>T_C$.

2.4 Interaction between Magnetic Moments on Lattice sites

Spontaneous magnetization of spinels can be estimated on the basis of their composition, cation distribution and the relative strength of the possible interaction. Since cation-cation distances are generally large, direct interactions are negligible. Because of the geometry of orbital involved, the strongest super exchange interaction is expected to occur between octahedral and tetrahedral cations. The strength of interaction or exchange force between the moments of the two metals ions on different sites depends on the distances between these ions and the oxygen ion that links them and also on the angle between the three ions. The interaction is greatest for an angle of 180^o and also where the interionic distances are the shortest. In the A-A and B-B cases, the angels are too small or the distances between the metal ions and the oxygen ions are too large. The best combination of distances and angles are found in A-B interactions. For an undistorted spinel, the A-O-B angles are about 125^o and 154^o [7]. The B-O-B angles are 90^o and 125^o but the latter, one of the B-B distances is large. In the A-A case the angle is about 80^o. Therefore, the interaction between moments on the A and B site is strongest. The BB interaction is much weaker and the most unfavorable situation occurs in the AA interaction.

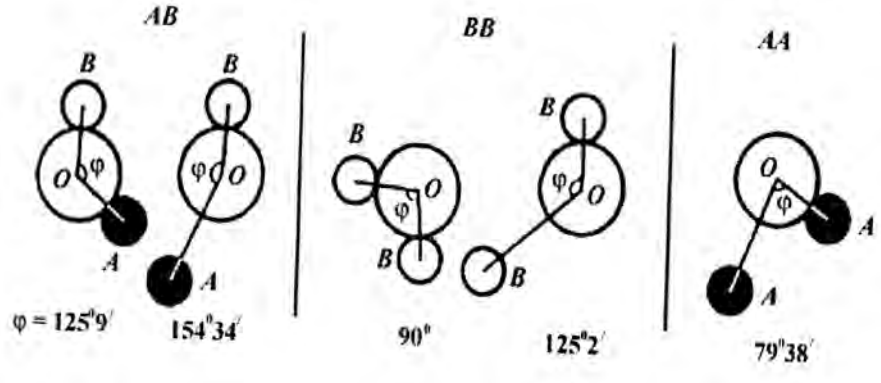

Fig.2.3. Interionic angles in the spinel structure for the different type of lattice site interactions**.**

2.5 Magnetism in Spinel Ferrite

The magnetic moment of a free atom is associated with the orbital and spin motions of electrons in an incomplete sub-shell of the electronic structure of the atom. In crystal the orbital motions are quenched, that is the orbital planes may be considered to be fixed in space relative to the crystal lattice, and in such a way that in bulk the crystal has no resultant moment from this source. Moreover this orbital-lattice coupling is so strong that the application of a magnetic field has little effect upon it. The spin axes are not tightly bound to the lattice as are the orbital axes. The anions surrounding a magnetic cation subject it to a strong inhomogeneous electric field and influence the orbital angular momentum. However, the spin angular momentum remains unaffected. For the first transition group elements this crystal field effect is intense partly due to the large radius of the 3d shell and partly due to the lack of any outer electronic shell to screen the 3d shell whose unpaired electrons only contribute to the magnetic moment. We have originally defined the magnetic moment in connection with permanent magnets. The electron itself may well be called the smallest permanent magnet [1]. For an atom a resulting spin quantum number S , the spin magnetic moment will be

$$\mu = g \bullet S(S+1)\mu_B$$

where g is the Lande splitting factor and μ_B is known as the Bohr magneton, is the fundamental unit of magnetic moment. The value of g for pure spin moment is 2 and the quantum number associated with each electron spin is ± ½. Fig. 2.4 illustrates the electronic configuration of Fe atoms and Fe^{3+} ions. Each unpaired electron spin produced 1 Bohr magneton. The moment of Fe atom and Fe^{3+} ion are $4\mu_B$ and $5\mu_B$ respectively.

$1s^2$	**$2s^2$**	**$2p^6$**	**$3s^2$**	**$3p^6$**	**$3d^6$**	**$4s^2$**	
••	••	•• •• ••	••	•• •• ••	•• • • • •	••	for Fe atom
••	••	•• •• ••	••	•• •• ••	• • • • •		for Fe^{3+} ion

Fig. 2.4. Electronic configuration of Fe atoms and Fe^{3+} ions

2.6 The Néel Theory of Ferrimagnetism

If we consider the simplest case of a two sublattice system having antiparallel and non-equal magnetic moments, the inequality may be due to:

i) different elements in different sites,

ii) same element in different ionic states, and

iii) different crystalline fields leading to different effective moments for ions having the same spin.

The spins on one sublattice are under the influence of exchange forces due to the spins on the second sublattice as well as due to other spins on the same sublattice. The molecular fields acting on the two sublattices A and B can be written as [3, 6-7]

$$\underline{H}_A = \lambda_{AA}\underline{M}_A + \lambda_{AB}\underline{M}_B$$

$$\underline{H}_B = \lambda_{AB}\underline{M}_A + \lambda_{BB}M_B$$

where $\underline{M}_A$ and $\underline{M}_B$ are the magnetizations of the two sublattices and λ's are the Weiss constants. Since the interaction between the sublattices is antiferromagnetic, λ_{AB} must be negative, but $_{AA}$ and $\bullet_{BB}$ may be negative or positive depending on the crystal structure and the nature of the interacting atoms. Probably, these interactions are also negative, though they are in general quite small. Assuming all the exchange interactions to be negative the molecular fields will be given by

$$\underline{H}_A = -\lambda_{AA}\underline{M}_A - \lambda_{AB}\underline{M}_B$$

$$H_B = -\bullet_{AB}\,\underline{M}_A - \bullet_{BB}\,\underline{M}_B$$

Since in general, λ_{AA} and $\bullet_{BB}$ are small compared to $\bullet_{AB}$, it is convenient to express the strengths of these interactions relative to the dominant $\bullet_{AB}$ interaction.

Let $\lambda_{AA} = \alpha\lambda_{AB}$

and $\lambda_{BB} = \beta\lambda_{AB}$

In an external applied field $\underline{H}$, the fields acting on A and B sites are

$$\underline{H}_A = \underline{H} - \lambda_{AB}(\alpha\underline{M}_A - \underline{M}_B)$$

$$\underline{H}_B = \underline{H} - \lambda_{AB}(\underline{M}_A - \beta\underline{M}_B)$$

At temperatures higher than the transition temperature, T_N, $\underline{H}_A$, $\underline{M}_A$ and $\underline{M}_B$ are all parallel and we can write

$$\underline{M}_A = \frac{C_A}{T}[\underline{H} + \lambda_{AB}(\alpha \underline{M}_A - \underline{M}_B)]$$
$$\underline{M}_B = \frac{C_B}{T}[\underline{H} - \lambda_{AB}(\underline{M}_A - \beta \underline{M}_B)], \qquad (2.1)$$

where C_A and C_B are the Curie constants for the two sublattices.

$$C_A = Nag\mu_B^2 S_A(S_A+1)/3K$$

and $C_B = N_{Bg}\mu_B^2 S_B(S_B+1)/3K$

N_A and N_B denote the number of magnetic ions on A and B sites respectively and S_A and S_B are their spin quantum numbers. Solving for the susceptibility, , one gets

$$\frac{1}{\chi} = \frac{T}{C} - \frac{1}{\chi_0} - \frac{\sigma}{T-\theta}, \qquad (2.2)$$

where C, χ_0 and θ are constants for a particular substance and are given by

$$C = C_A + C_B$$

$$\frac{1}{\chi_0} = -\frac{1}{C^2}\left[C_A^2\lambda_{AA} + C_n^2\lambda_{BB} + 2C_AC_B\lambda_{AB}\right]$$

$$\sigma = \frac{C_AC_B}{C^3}\left[C_A^2(\lambda_{AA}-\lambda_{BB})^2 + C_B^2(\lambda_{BB}-\lambda_{AB})^2\right]$$
$$-2C_AC_B\{\lambda^2_{AB} - (\lambda_{AA}+\lambda_{BB})\lambda_{AB} + \lambda_{AA}\lambda_{BB}\}$$

$$\theta' = -\frac{C_AC_B}{C}(\lambda_{AB}+\lambda_{BB}) - 2\lambda_{AB}$$

The equation (2.2) for $\frac{1}{\chi}$ is a hyperbola and is the characteristic which differentiates ferrimagnets and ferromagnets. The paramagnetic Curie temperature T_c is obtained from equations (2.1) with H = 0 and setting the determinant of the coefficients of M_i equal to zero. This gives

$$T_c = \frac{1}{2}\left[C_A\lambda_{AA} + C_B\lambda_{BB} + \{(C_A\lambda_{AA} - C_B\lambda_{BB})^2 + 4C_AC_B\lambda^2_{AB}\}^{\frac{1}{2}}\right] \qquad (2.3)$$

Though the simple Neel theory successfully explains the observed magnetic moments and temperature dependences of the magnetization of large number of ferrites, it fails for some cases.

i) Some of the M vs. T curves have finite slopes at 0K, which can not be explained on Neel's theory without violating the third law of thermodynamics.

ii) The essential requisite for Neel configuration is a strong negative exchange interaction between A and B sublattices which results in their being magnetized in opposite directions below the transition point. But there may be cases where intrasublattice interactions are comparable with intersublattice interaction. Neel's theory predicts paramagnetism for such substances at all temperatures. This is unreasonable since strong AA or BB interaction may lead to some kind of ordering especially at low temperature. In the cases of no AB interaction, antiferromagnetic ordering may be expected either in the A or in the B sublattice.

iii) The spontaneous magnetization of a number of ferrites is significantly lower than predicted by the Neel's theory. These failures are due to the over simplifications included in the model: (1) only two sublattices were considered instead of six (six cations in the primitive cell), and (2) the magnetic moments in each sublattice were a priori assumed to be parallel.

2.7 Hysteresis

The state of magnetization of a solid is a function of the strength and direction of the magnetizing field. If we consider a ferromagnetic material which contains many small magnetic domains but no net magnetization, we can examine what happens to the domains as the field strength is increased . As the field is increased from zero, the effect on the solid is to displace domain boundaries in a reversible fashion. If the magnetic field is switched off, the domain boundaries return to their starting positions. Thus the initial part of the B-H curve results from reversible domain boundary displacement and the slope is called initial permeability $\mu_{i.}$ As the magnetic field strength is increased there is an irreversible boundary displacement and at first the induced magnetization increases more rapidly and gives a maximum slope μ_{max}. Finally in the upper part of the magnetization curve all domain boundaries have been displaced and further increase in the magnetic field cause rotation of the domains in the direction of the applied field. At this point the material is saturated , higher fields cannot induce more magnetization.

As the magnetic field is decreased to zero, the induced magnetization does not decrease to zero but the alignment of most of the domains during magnetization results in a remanent magnetization or remanance B_r. When the direction of the magnetic field is reversed the induced magnetization decreases and finally becomes zero at a value of the magnetic field strength called the coercive force H_C. Further increased magnetic field strength in this opposite direction eventually causes magnetic saturation in the reverse direction and produces a saturation B_S and remanence B_r values of the same magnitude as in the first quadrant. As an applied field is cycled from one direction to the other direction, the Hysteresis loop is followed. Since the area of the Hysteresis loop represents the energy or work to bring about changes in the magnetic domain structure, the product BH, called the energy product, represents a net loss in the system, usually in the form of heat. A material with a low coercivity is said to be soft and may be used in microwave devices, magnetic shielding, transformers or recording heads. Magnetic materials with high coercivity are called hard and are used to make permanent magnets. Permanent magnets fine application in electric motors and magnetic recoding media.

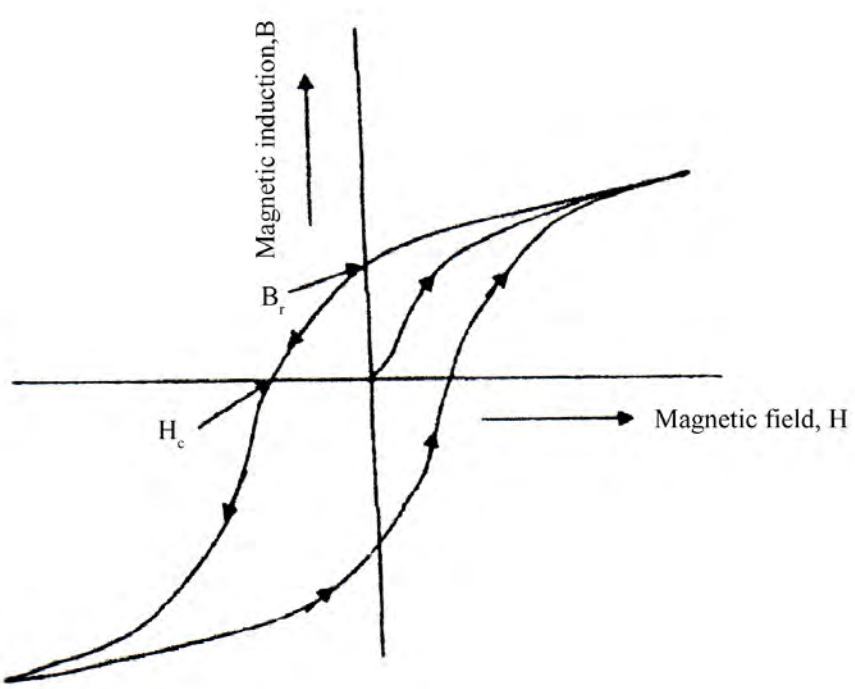

Fig. 2.5. Magnetization characteristic and Hysteresis loop.

References:

[1] M. A. Wahab, *Solid State Physics: Structure and Properties of Materials*, Narosa Publishing House, New Delhi (1999)

[2] A. Goldman, *Handbook of Modern Ferromagnetic Materials*, Kulwer Acad. Pub, Boston, U.S.A (1999)

[3] B. D. Culity, *Introduction to Magnetic Materials*, Addison-Wisley Publishing Company, Inc., California (1972)

[4] R.Valenzuela, *Magnetic Ceramics, Cambridge University Press,* Cambridge (1994)

[5] F. Brailsford, *Physical Principles of Magnetism, D. van Nostrand Company* Ltd., London(1996)

[6] A. J.Dekker, *Solid State Physics, Macmillan, India Ltd*., New Delhi (1998).

[7] S. Chikazumi, *Physics of Magnetism, Jhon Wiley & Sons, Inc*., New York(1966)

.

CHAPTER THREE

Methodology of Ferrite Preparation

3.1 Solid State Reaction Method

A goal common to all the ferrites is the formation of the spinel structure. Now a days, the majority of ferrite powders are made by the conventional ceramic process or Solid State Reaction technique. The normal methods of preparation of ferrites comprise the conventional ceramic method or powder metallurgy, chemical co-precipitation method, sol-gel method, spray-drying etc.[1-2]. In this thesis work conventional ceramic method has been employed for the preparation of $Li_{0.5-x/2}\ Cu_xFe_{2.5-x/2}O_4$, where x = 0 to 1, ferrite for its relative simplicity and availability.

In the solid state reaction method, the required composition is usually prepared from the appropriate amount of raw mineral oxides or carbonates by crushing, grinding and milling. The most common type of mill is the ball mill. Milling can be carried out in a wet medium to increase the degree of mixing. This method depends on the solid state inter-diffusion between the raw materials. The extend of the work in this step varies greatly, depending on the starting materials. When component oxides are used, the corresponding step involves a mere mixing of the oxides by wet milling. To avoid iron contamination, mixing is done with stainless steel balls in a steel ball milling machine and a fluid such as distilled water or acetone/ethanol is used to prepare the mixture into slurry. The raw materials for the preparation of $Li_{0.5-x/2}\ Cu_xFe_{2.5-x/2}O_4$ ferrite were oxides of iron, lithium and copper. The constituent in required stoichiometric proportions were weighed first and then thoroughly mixed using ceramic mortar and pestle. The resultant powder was then ball milled for 6 hours to produce fine powders of mixed constituents.

Solids do not usually react at room temperature over normal time scales. Thus it is necessary to heat them at higher temperatures for the diffusion length $(2Dt)^{1/2}$ to exceed the particle size, where D is the diffusion constant for the fast diffusing species and t is the firing time. The slurry prepared is dried, palletized and then transferred to a porcelin crucible for prefiring at temperature 800°C. This was performed in a furnace named Gallen Camp at Materials Science Division, AECD. The calcined powders are again crushed into fine powders. The pellets or toroid shaped samples are prepared from these calcined powders using die-

punch assembly or hydrostatic or isostatic pressure. Sintering is carried out in the solid state , at temperature ranging 1100-1200^{o}C. in air for 3-4 hours.[3-4]

The general solid state reaction leading to a ferrite may be represented as

$MeO + Fe_2O_3 \rightarrow MeFe_2O_4$ *(spinel)*

where *Me* is the divalent ions.

During the prefiring stage, the reaction of Fe_2O_3 with metal oxide (say, MeO or Me'_2O_3) takes place in the solid state to form spinel according to the reactions [5]

$2\,Me'_2O_3 + 4Fe_2O_3 \rightarrow 4\,Me'Fe_2O_4$ *(spinel)* $+O_2$

The Li_2O and CuO are creeps into Fe_2O_3 as below, to form an intermediate phase

$2Fe_2O_3 + Li_2O \rightarrow 2LiFe_2O_4$

$Fe_2O_3 + CuO \rightarrow CuFe_2O_4$

After that Cu ions are introduced by

$Li_{0.5-x/2}\,O + x.CuO + Fe_{2.5-x/2}O_4 \rightarrow Li_{0.5-x/2}Cu_xFe_{2.5-x/2}O_4$

Block Diagram

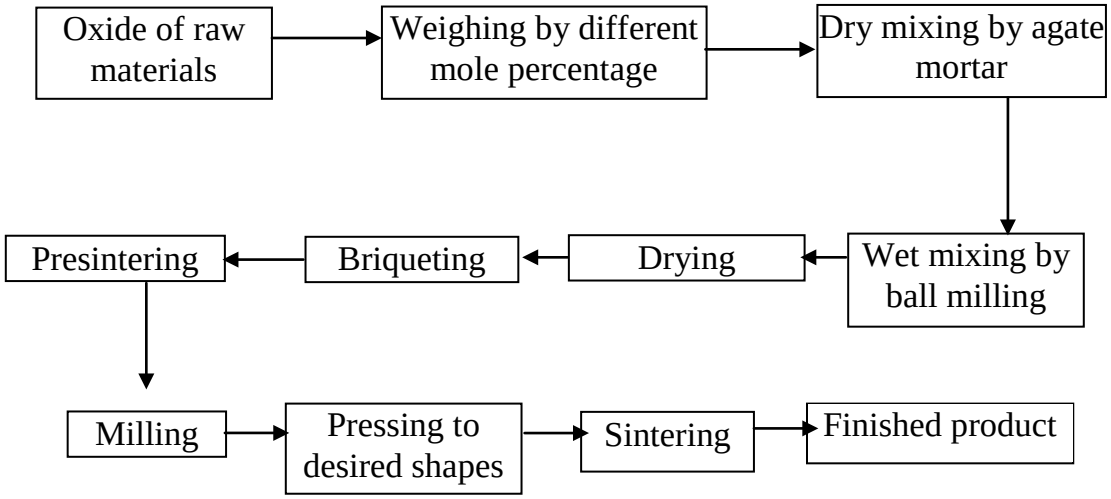

As a whole the preparation procedure generally consists of four major steps:

i) Preparing a mixture of materials with the cations in the ratio corresponding to that in the final product.

ii) Prefiring the mixture to form ferrite.

iii) Converting the 'raw' ferrite into powder and pressing the powder into the required shapes.

iv) Sintering to produce a highly densified product.

3.2 Sintering

Sintering is defined as the process of obtaining a dense, tough body by heating a compacted powder for a certain time at a temperature high enough to significantly promote diffusion, but clearly lower than the melting point of the main component. The driving force for sintering is the reduction in surface free energy of the powder. Part of this energy is transferred into interfacial energy in the resulting polycrystalline body [2, 6] The sintering time, temperature and the furnace atmosphere play very important role on the magnetic property of ferrite materials. *As* the final major step in the preparation of ferrite product, sintering must fulfill three requirements:

(i) To bond the particles together so as to impart sufficient strength to product.

(ii) To dense the grain compacts by elimination the pores and

(iii) To homogenize the materials by completing the reactions left unfinished in the prefiring step.

Sintering of crystalline solids follows the following empirical relationship regarding rate of grain growth [7]:

$$d = k\, t^{a}$$

where d is the mean grain diameter, t is sintering time, a is about 1/3 and k is a temperature dependent parameter. Sintering is divided into three stages [8].

Stage 1: Contact area between particles increases

Stage 2: Porosity changes from open to closed porosity

Stage 3: Pore volume decreases, grains grow.

References :

[1] A. Goldman, *Handbook of Modern Ferromagnetic Materials, Kulwer Acad. Pub*, Boston, U.S.A (1999)

[2] R.Valenzuela, *Magnetic Ceramics, Cambridge University Press, Cambridge* (1994)

[3] R. J. Brook, *Sintering: An Overview , Concise Encyclopedia of Advanced Ceramic Materials, Pergamon Press,* Oxford, p 438, (1991)

[4] P. Reijnen, *Science of Ceramics, Academic Press,* London (1967)

[5]P. I. Slick, *Ferrites for Non-microwave Applications*, 2, North Holand Pub. Co. (1980)

[6] W.D. Kingery, H. K. Bowen and D. R. Uhlman, *Introduction to Ceramics, 2nd edition, Wiley Intersciences*, Newyork, p 476 (1976)

[7] R. L. Coble and J. E.Burke, *4th Int. Symp. On the Reactivity of Solids, Amsterdam*, p 38-51, (1960)

[8] I. J. McColm and N. J. Clark, *Forming, Shaping and Working of high Performance Ceramics, Blackie*, Glasgow, p1-338, (1988)

CHAPTER FOUR

Experimental Measurements

4.1 The X-ray Diffraction

The X-ray diffraction (XRD) provides precise knowledge of the lattice parameter as well as the substantial information on the crystal structure of the material under study. XRD is one of the most effective tools for the determination of phase in a sample. X-rays are the electromagnetic waves whose wavelengths are in the neighborhood of 1• . The wavelength of an X-ray is thus of the same order of magnitude as the lattice constant of crystals.

Whenever X-rays are incident on a crystal surface, they are reflected from it. This is called Bragg reflection. If a beam of monochromatic radiation of wavelength • incident on a periodic crystal plane at an angle • and is diffracted in the same angle, this event abides by the celebrated Bragg's law which is given below

$$2d \sin\theta = n\lambda \tag{4.1}$$

Here d is the distance between crystal planes, and n is positive integer. Bragg's law also suggests that the diffraction is only possible when • <2d [1]

X-ray diffraction (XRD) is a versatile non-destructive analytical technique for identification and quantitative determination of various crystalline phases of powder or solid samples of any compound. A PHILIPS X Pert PRO X-ray diffraction system was used to get X-ray data for the samples at the Materials Science Division, Atomic Energy Center, Dhaka, which is a sophisticated X-ray diffractometer installed very recently. The powder diffraction technique was used with a primary beam power of 40 kV and 30mA for Cu radiation. A nickel filter was used to reduce Cu-K_a radiation and finally Cu-K_a radiation was only used as the primary beam. A (θ- 2θ) scan was taken from 15° to 75° to get possible fundamental peaks of the sample with the sampling pitch of 0.02° and time for each step data collection was 1.0 sec. Both the programmable divergence and receiving slits were used to control the irradiated beam area and output intensity from the sample respectively. An anti-scatter slits were used just after the sample holder to reduce air scattering. Two solar slits were used just after the tube and in front of the detector to get parallel beam only. Data was analyzed using computer software "X PERT HIGHSCORE".

4.1.1. Interpretation of the XRD Data :

The XRD data consisting of $\bullet_{hkl}$ and d_{hkl} values corresponding to the different crystallographic planes are used to determine the structural information of the samples like lattice parameter and constituent phase.

The lattice parameter for each peak of each sample was calculated by using the formula:

$$a = d_{hkl} \times \sqrt{h^2 + k^2 + l^2} \tag{4.2}$$

where h, k and l are the indices of the crystal planes. To determine the exact lattice parameter for each sample, Nelson-Riley method was used. The Nelson-Riley function F($\bullet$), can be written as

$$F(\theta) = \frac{1}{2}\left(\frac{\cos^2\theta}{\sin\theta} + \frac{\cos^2\theta}{\theta} \right) \tag{4.3}$$

Now drawing the graph of 'a' vs F(θ) and using linear fitting of those points will give us the lattice parameter a_0. This is the value of 'a' at F(θ) =0.

4.1.2 X- Ray density and bulk density determination:

X-ray density $\bullet_x$ was also calculated using the lattice parameter. The relation between $\bullet_x$ and a is as follows:

$$\rho_x = \frac{8M}{Na^3}\, g/cm^3 \tag{4.4}$$

where N is the Avogadro's number (6.02×10^{23} mol^{-1}), M is the molecular weight.

The bulk density, ρ_B is measured by the formula [2],

$$\rho_B = \frac{M}{V} \tag{4.5}$$

where M is the mass of the disc sample and V its volume.

Porosity (P) in percentage was calculated using the

$$P = \left(1 - \frac{\rho_B}{\rho_x}\right) \times 100\% \tag{4.6}$$

4.2 The study of microstructure

Sensitivity of electrical and magnetic properties depend on the microstructure of the ferrite sample. Permeability is directly proportional to grain size, At least up to a critical diameter of the grains permeability increases monotonically. Density and resistivity depends on the porosity of the sample. So study of microstructure is necessary for making prediction about the result of permeability and resistivity. The SEM microstructure of samples sintered at 1100^{o}C were studied by Scanning Electron Microscope. To observe the microstructure, the ferrite samples were polished with fine Al_2O_3 powder followed by thermal etching from 800-900^{o}C for all samples. When the etching was completed, the grains were seen clearly by the SEM. The average grain size was calculated by the linear intercept method.

4.3 Curie Temperature (T_c) Measurement

Curie temperature measurement is one of the most important measurements for magnetic materials. Curie temperature provides substantial information on magnetic states of a substance in respect of the strength of exchange interaction. So, the determination of Curie temperature accurately is of great importance. Curie temperature measurements were done by using Agilent precision impedance analyzer (Agilent 4294A), with a small oven and a thermocouple based thermometer. The temperature dependent permeability was measured by using induction method. The specimen formed the core of the coil. We used a 100 kHz AC signal of 100 mV. By varying temperature, inductance of the coil as a function of temperature was measured. Dividing this value by L_o (inductance of the coil without core material), permeability of the sample was determined. When the magnetic state inside the ferrite sample changes from ferromagnetic to paramagnetic, the permeability falls sharply. From this sharp fall at specific temperature, the Curie temperature is determined. This is the basic principle used in our experimental set up. The number of turns in each coil is 5. The sample thus wound is kept in the middle position of a tubular oven with a thermocouple placed close to the sample. The thermocouple measures the temperature inside oven and also of the sample. The sample is kept just in the middle part of the cylindrical oven so that temperature gradient is minimized. The temperature of the oven is raised slowly. If the heating rate is very fast then

temperature of the sample may not follow the temperature inside the oven and there can be misleading information on the temperature of the samples. So, a slow heating rate can eliminate this problem. Also a slow heating ensures accuracy in the determination of Curie temperature. The oven was kept thermally insulated from the surroundings. Actually Curie Temperature was measured from the temperature dependence of initial permeability.

4.4 Saturation Magnetization Measurement

Magnetization is defined as the magnetic moment per unit volume. There are various techniques of measuring magnetization of a substance. In the present thesis saturation magnetization has been measured by a vibrating sample magnetometer (VSM) at room temperature. These measurements were carried out in Department of Physics, Bangladesh University of Engineering and Technology (BUET), Dhaka. Vibrating sample magnetometer, as the name implies, vibrate the sample as part of the measurement process. This provides the flux meter element of the system with the dynamic component which it requires to make the measurement. The applied field is changed so, at each measurement point the field is static and hence no eddy currents to cause problems. The objective when using a VSM or any other type of magnetic characterization system is to obtain the dependence of the magnetization on the applied field. The sample, usually a sphere or small disc, is cemented to the lower end of a rod, the other end of which is fixed to a mechanical vibrator. Current through the vibrator and vibrate the rod at about 37 Hz with amplitude of about 7 V in a direction at right angles to the magnetic field. The oscillating magnetic field of the sample induces an alternation emf in the direction coils. The vibrating rod also carries a reference specimen, in the form of a small permanent magnet near its upper end, the oscillating field of this induces another emf in two reference coils. The two voltage form two sets of coils are compared, and the difference is proportional to the magnetic moment of the sample. The magnetization measurement was performed (0- 1500 G) magnetic field for all samples.

Figure 4.1: Vibrating Sample Magnetometer

4.4.1 Calibration of the VSM

The calibration of the VSM was done by using a 152mg spherical sample of 99.99% pure nickel. The sample was made spherical with the help of the sample shaping device. The saturation magnetic moment of the sample has been calculated using available data. The ratio transformer reading is obtained by actual measurement from the relation

$$M = K K^{/} \tag{4.7}$$

where M is magnetic moment, $K^{/}$ is saturation ratio transformer reading and K is VSM calibration constant. But

$M = m \bullet$ (4.8)

where, • is the specific magnetization and m is the mass of the sample. From (4.7) and (4.8) calibration constant is given by

$K = m \bullet / K^{/}$ (4.9)

Calibration Data

(i) Sensitivity =100μV

(ii) Reference phase =89.9°

(iii) Time constant =1sec

(iv) Peak to peak voltage = 7 V

(v) Bandwidth =12 dB

(vi) Reference frequency, f = 37 Hz

(vii) Mass of the pure nickel sample, m =152 $x10^{-6}$ kg

(viii) Bohr magneton, s = 58.5 Am^2/kg

(ix)) Ratio transformer reading, $K^{/}$ = 5.05V

Therefore,

$K = 152 \times 10^{-6} \times 58.5 / 5.05$

$= 1.760$ emu / V

The magnetization of the samples were calculated by using the following

$$M = \frac{KV}{m} \quad \text{emu /g} \qquad (4.10)$$

where, M = Magnetization of the experimental sample

m = Mass of the experimental sample

V = Voltage correspond to the magnetization

K = Calibration constant of the VSM.

4.5 Complex Permeability Measurement

For high frequency application, the desirable properly of a ferrite is the high permeability with low loss. The present goal of most of the recent ferrite researchers is to fulfill this requirement. Before going into the complexity of permeability measurement, we take a detour through the theories and mechanisms involved in permeability.

Permeability is namely defined as the proportional constant between the magnetic field induction B and applied field intensity H [3-4]:

$$\mathbf{B} = \mu \mathbf{H} \tag{4.11}$$

If a magnetic material is subjected to an AC magnetic field as given below;

$$\mathbf{H} = \boldsymbol{H_0 e^{iwt}} \tag{4.12}$$

then it is observed that the magnetic flux density B experiences a delay. This delay is caused due to presence of various losses and is thus expressed as

$$\boldsymbol{B = B_0 e^{i(wt-\bullet)}} \tag{4.13}$$

where δ is the phase angle and marks the delay of B with respect to H. The permeability is then given by

$$\mu = \frac{B}{H} = \frac{B_0 e^{i(\varpi t - \delta)}}{H_0 e^{i\varpi t}}$$

$$= \frac{B_0 e^{-i\delta}}{H_0} = \mu' - i\mu'' \tag{4.14}$$

$$\text{where, } \mu' = \frac{B_0}{H_0}\cos\delta, \mu'' = \frac{B_0}{H_0}\sin\delta \tag{4.15}$$

The real part μ' of complex permeability μ as expressed in equation (4.11) represents the component of B which is in phase with H, so it corresponds to the normal permeability. If there are no losses, we should have $\mu = \mu'$. The imaginary part μ'' corresponds to that part of B which is delayed by phase angle ranging upto 90° from H. The presence of such a

component requires a supply of energy to maintain the alternating magnetization, regardless of the origin of delay. The ratio of $\mu''to\mu'$, as is evident from equation (4.11) gives

$$\frac{\mu''}{\mu'} = \frac{(B_0/H_0)\sin\delta}{(B_0/H_0)\cos\delta} = \tan\delta \tag{4.16}$$

This $\tan\delta$ is called the Loss Factor or Loss tangent. The Q-factor or quality factor is defined as the reciprocal of this loss factor, i.e.

$$Q = \frac{1}{\tan\delta} \tag{4.17}$$

4.5.1 Techniques of measurements of permeability

Measurements of permeability normally involve the measurements of the change in self inductance of a coil in presence of the magnetic core. The behaviour of a self inductance can now be described as follows. Suppose we have an ideal lossless air coil of inductance L_o. On insertion of magnetic core with permeability μ, the inductance will be L_0. The complex impedance Z of this coil [5] can be expressed as

$$Z = R + jX = j\varpi L_0 \mu = j\bullet L_o (\mu^{/} - j \mu^{//}) \tag{4.18}$$

where the resistive part is

$$R = \varpi L_o \mu^{/} \tag{4.19}$$

and the reactive part is

$$X = \bullet L_o \mu^{//} \tag{4.20}$$

The radio frequency (RF) permeability can be derived from the complex impedance of a coil Z (equation 4.14). The core is usually toroidal to avoid demagnetizating effects. The quantity Lo is derived geometrically.

4.5.2 Measurement of frequency characteristics of Li-Cu ferrite :

The frequency characteristics of the Li-Cu ferrite samples i.e. the permeability spectra were investigated using a Hewlett Packard Impedance Analyzer of model 4192A. The measurements of inductances were taken in the frequency range of 1 kHz to 13 MHz. The values of measured parameters such as inductance and loss tangent were obtained as a function of frequency. The real and the imaginary part of permeability are calculated. μ' is calculated by using the following formula:

$$L_s = L_0 \mu' \tag{4.21}$$

and $$\tan\delta = \mu'' / \mu' \tag{4.22}$$

where L_s is the self-inductance of the sample core and

$$L_0 = \frac{\mu_0 N^2 s}{\bar{d}} \tag{4.23}$$

where L_0 is the inductance of the winding coil without the sample core and N is the number of turns of coil (here N = 5), S is the area of cross section of the toroid as given below

s = dh,

where, d = $(d_1 \sim d_2) / 2$,

h = height

and $\bar{d}$ is the mean diameter of the sample given as follows

$$\bar{d} = \frac{d_1 + d_2}{2} \tag{4. 24}$$

4.6 Electrical Resitivity Measurement:

Electrical resistivity of the samples have been measured by two probe method. Samples were prepared by sintering temperature of 1100^{o}C . The samples were polished with the help of emery paper with grit size 600 and 800 successively. Then silver past was added to the both sides of the polished samples together with two thin copper wires of 100 micron diameter. The resistivity was measured using an Electrometer Keithley model 6514 at room and higher temperatures. The resistivity has been calculated using the formula

$$R = \rho \, l / A \tag{4.25}$$

where ρ is the resistivity , l and A are the thickness and the area of the sample respectively.

4.7 Determination of Activation Energy

Ferrites are semiconductors and their resistivity decreases with increasing temperature according to the relation

$$\rho = \rho_o \exp(E_P / kT) \tag{4.26}$$

where E_P is an activation energy which , according to [6] is the energy needed to release an electron from the ion for a jump to the neighbouring ion, so giving rise to electrical conductivity and k is the Boltzmann's constant.

In most cases, a straight line is found in a wide temperature range, with a slope corresponding to E_P according to the relation

$$E_p = 0.198 \times 10^{-3} \times d (\log \rho) / d(1/T) \tag{4.27}$$

4.8 Dielectric constant measurement

The simplest capacitor structure is a pair of parallel conducting plates separated by a medium called the dielectric. The value of the capacitance between the plates is given by the equation

$$C = \varepsilon \times A / d \tag{4.28}$$

where A is the area of the plates

d is the separation between the plates

ε is the absolute permittivity of the dielectric, which is a measure of the electrostatic energy stored within it and therefore dependent of the material.

The dielectric constant of an insulating material is therefore numerically the ratio of the capacitance of a capacitor containing that material to the capacitance of the same electrode system with vacuum replacing the insulation as the dielectric medium.

The dielectric constant of the medium (also known as the relative permittivity) is defined as

$$\varepsilon_r = \varepsilon / \varepsilon_o \tag{4.29}$$

where ε_o is the permittivity of free space, which has value of 8.85×10^{-12} Fm^{-1}

References:

[1] C. Kittel, *Introduction to Solid State Physics, 7th edition*, Jhon Wiley & Sons, Inc., Singapore (1996)

[2] B. D. Cullity, *Introduction to Magnetic Materials*, Addison-Wisley Publishing Company, Inc., California (1972)

[3] S. Chikazumi, *Physics of Magnetism*, Jhon Wiley & Sons, Inc., New York (1966)

[4] D. Hadfield, Permanent Magnets and Magnetism, Jhon Wiley & Sons, Inc., New York (1962)

[5] A. Goldman, *Handbook of Modern Ferromagnetic Materials*, Kulwer Acad, Pub, Boston, U.S.A (1999)

[6] E. J. W. Verwey, and J. H. de Boer, Rec. Cation Arrangement in a Few Oxides with Crystal Structures of the Spinel Type trav. Chim Pays Bas, 55, 531-540 (1936)

CHAPTER FIVE

Results and Discussion

5.1 X-ray Diffraction (XRD):

The X-ray diffraction patterns of $Li_{0.5-x/2}Cu_xFe_{2.5-x/2}O_4$ samples sintered at 1000°C for 3 hours is shown in Fig. 5.1. It is observed from Fig 5.1(a) that the samples in the range of $0 \leq x \leq 0.3$ are cubic spinel. Tetragonality begins from the composition of x = 0.4 to 0.8 as has been manifested by twin peak in the XRD patterns. For the composition of x = 0.9 and 1.0 are presented in Fig 5.1(b), it was found that tetragonality disappeared at 1000°C. For the sintering temperature of 800°C, and x = 0.9 and 1.0 both the samples showed ideal tetragonal structure as has been presented in Fig. 5.1 (b). To study the variation of tetragonality with sintering temperature, the samples were sintered at 1100°C. At the sintering temperature of 1100°C the samples were again of cubic spinel structure. It is widely known that tetragonality is very much dependent on sintering temperature and higher concentration of cooper. At 1100^oC, x-ray diffraction pattern reveals apparent transformation to cubic structure though some tetragonality may persist even at higher sintering temperature for higher copper content. The XRD patterns for $Li_{0.5-x/2}Cu_xFe_{2.5-x/2}O_4$ sintered at 1100^oC are shown in Fig. 5.2 to 5.9. Analyzing the XRD patterns, the observed peak at (220), (311), (400), (422), (511) and (440) confirmed the spinel structure of the samples. The sharp peaks indicate that the samples are in good crystalline form.

In order to find the experimental lattice parameter, Nelson-Riley (N-R) function F(•) is used. For the calculation of the exact lattice parameter, the graph of apparent lattice parameter 'a' vs N-R function F(•) are plotted in the Fig 5.10 to 5.11. The Y-axis values at F(•) = 0 give the exact values of lattice parameters. The equations of the linear fitting of the points are shown in the graphs. The variation of lattice parameters 'a' with composition 'x' are plotted for the sintering temperature of 1100^oC and 1200^oC that are shown in Fig 5.12, it is observed that the lattice parameter increases with the increase of Cu content. This behaviour can be attributed to the replacement of Fe^{3+} (0.64 •) and Li^+ (0.68 •) by Cu^{2+} (0.72 •) ion [1]. It does not follow Vegards law [2] properly, because of the structural change at higher Cu

content and higher sintering temperature. In Table 5.1, lattice parameters have been presented for different compositions in the sintering temperature of 1100°C and 1200°C.

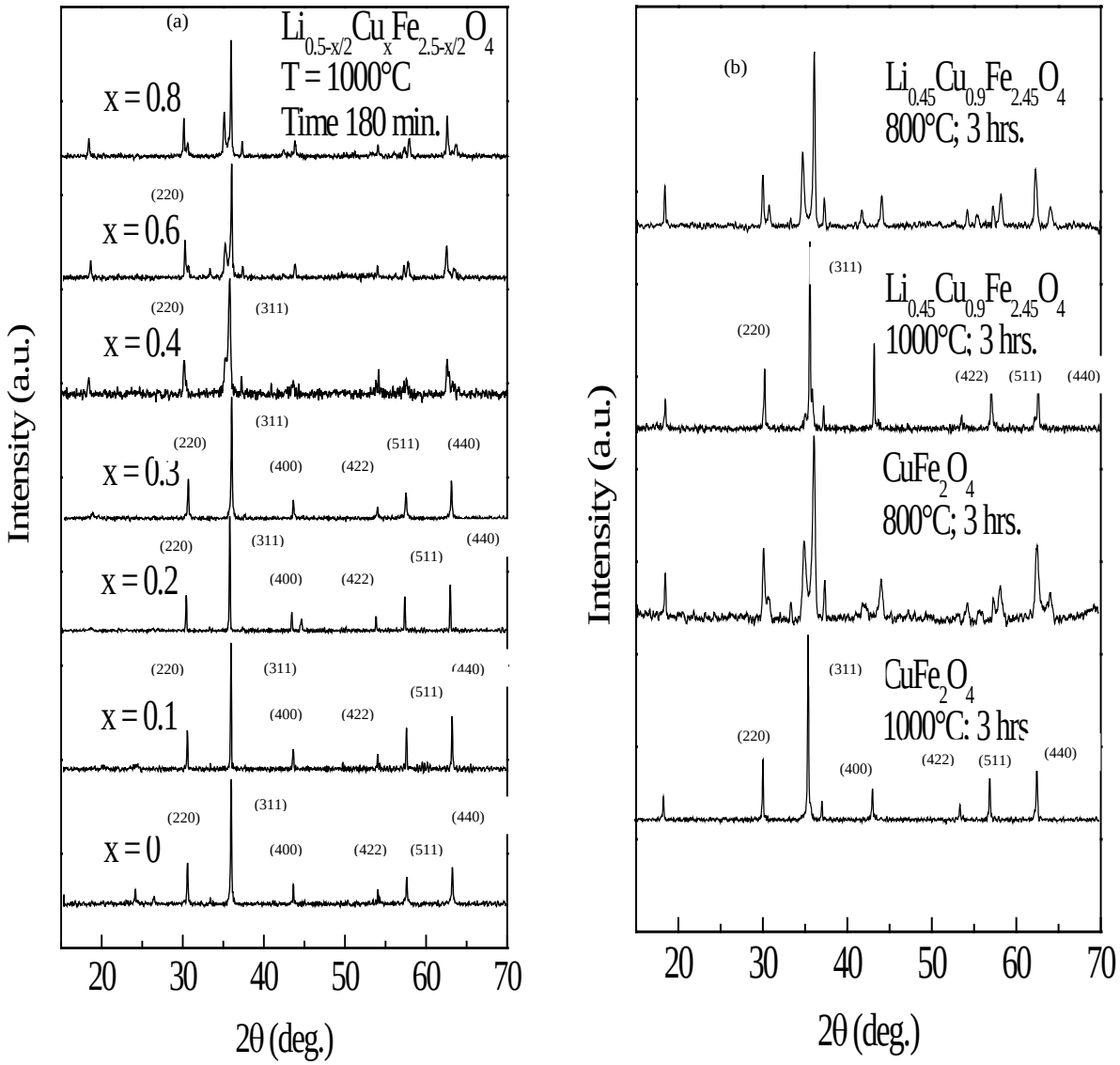

Fig. 5.1 XRD patterns of $Li_{0.5-x/2}Cu_xFe_{2.5-x/2}O_4$, sintered at 1000°C for 3 hrs.

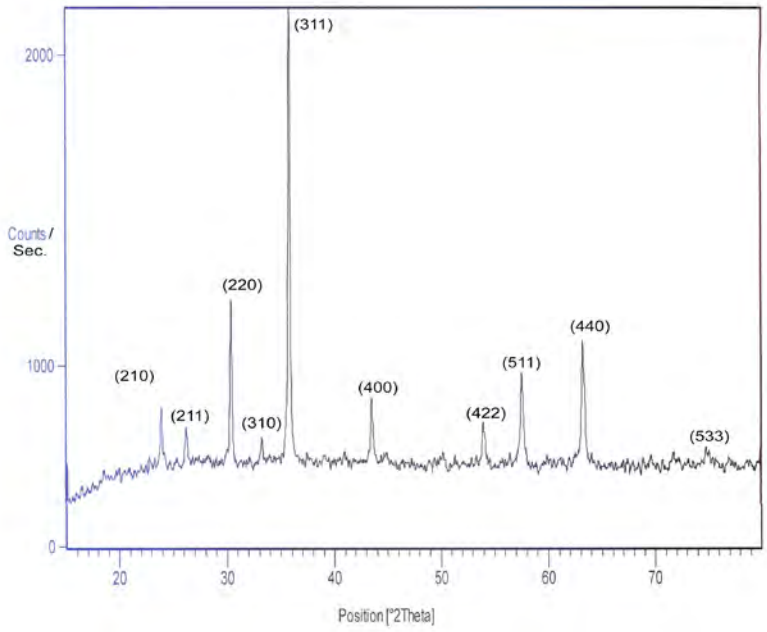

Fig. 5.2. XRD pattern for $Li_{0.5-x/2}Cu_xFe_{2.5-x/2}O_4$ with x = 0 sintered at 1100^0C**.**

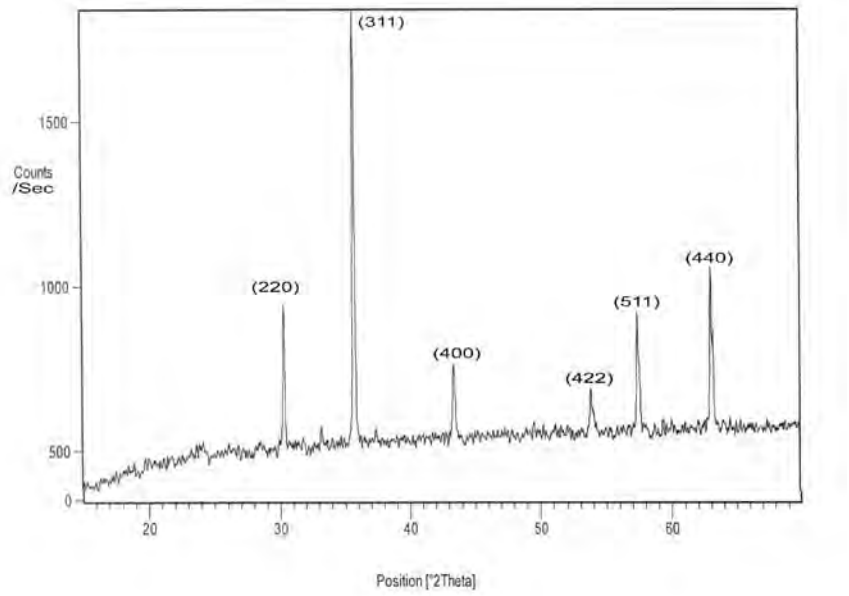

Fig. 5.3. XRD pattern for $Li_{0.5-x/2}Cu_xFe_{2.5-x/2}O_4$ with x = 0.1 sintered at 1100^0C

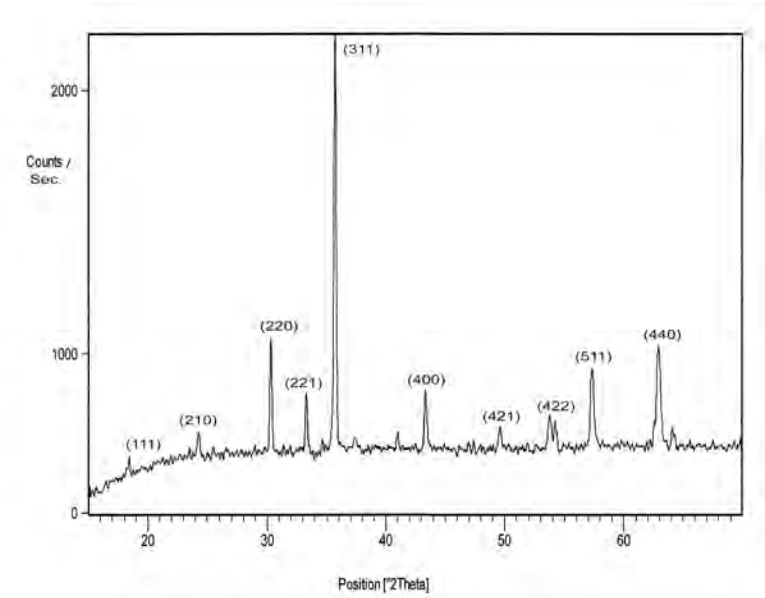

Fig. 5.4. XRD pattern for $Li_{0.5-x/2}Cu_xFe_{2.5-x/2}O_4$ with x = 0.3 sintered at 1100^0C

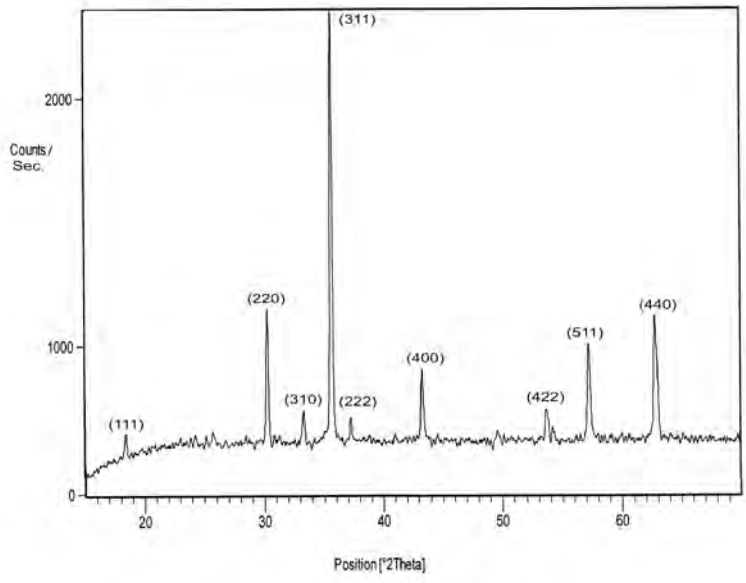

Fig. 5.5. XRD pattern for $Li_{0.5-x/2}Cu_xFe_{2.5-x/2}O_4$ with x = 0.4 sintered at 1100^0C

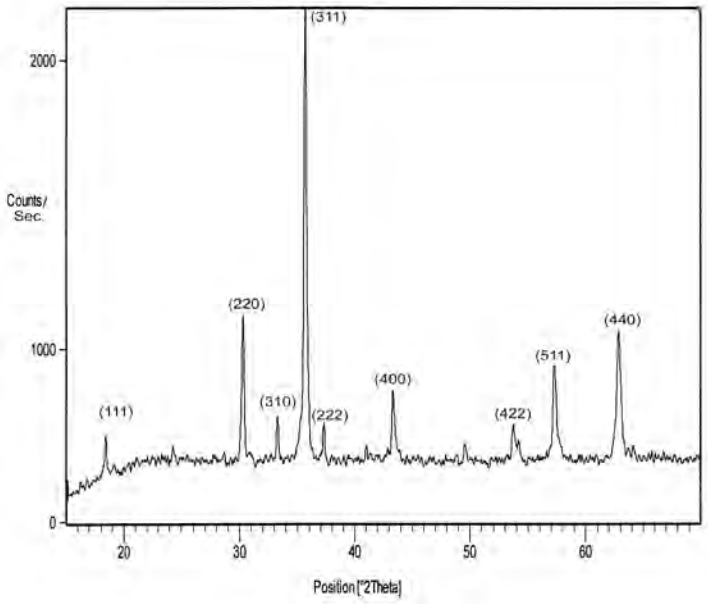

Fig. 5.6. XRD pattern for $Li_{0.5-x/2}Cu_xFe_{2.5-x/2}O_4$ with x = 0.5 sintered at 1100^0C

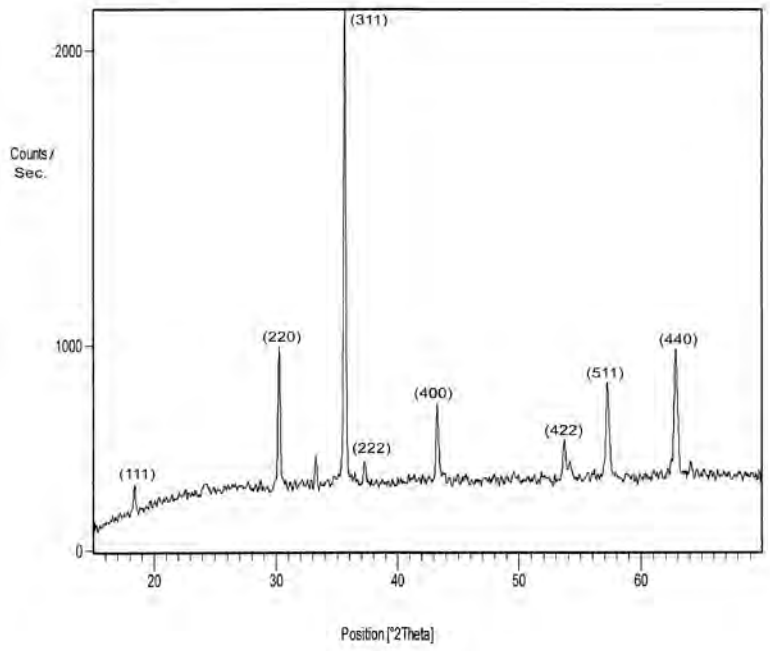

Fig. 5.7. XRD pattern for $Li_{0.5-x/2}Cu_xFe_{2.5-x/2}O_4$ with x = 0.7 sintered at 1100^0C

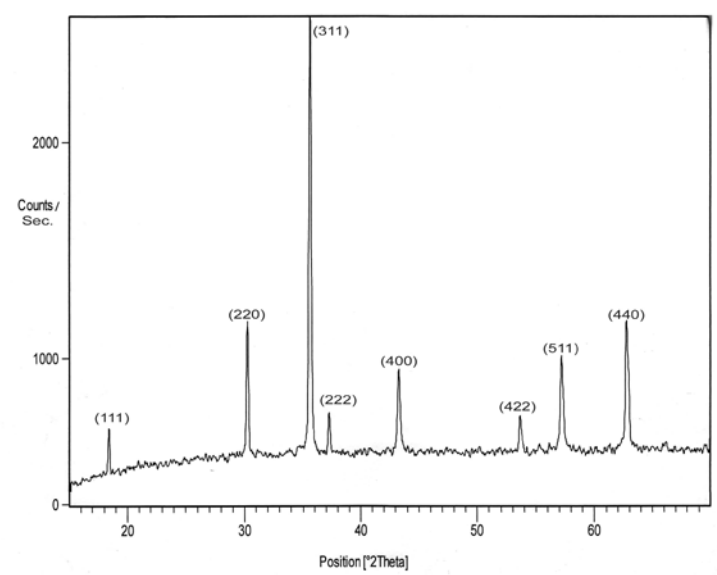

Fig. 5.8. XRD pattern for $Li_{0.5-x/2}Cu_xFe_{2.5-x/2}O_4$ with x = 0.9 sintered at 1100^oC

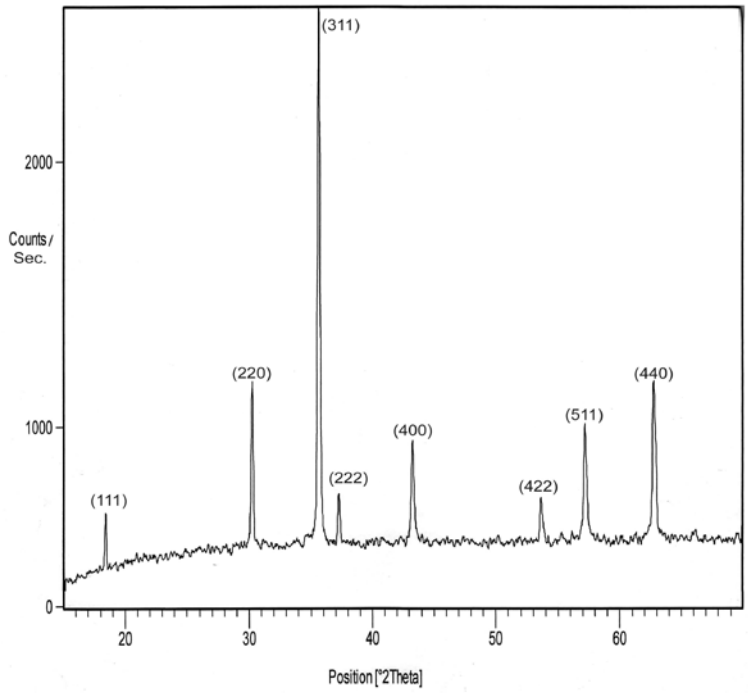

Fig. 5.9. XRD pattern for $Li_{0.5-x/2}Cu_xFe_{2.5-x/2}O_4$ with x = 1.0 sintered at 1100°C

Plot of N-R function in the sintering of 1100°C :

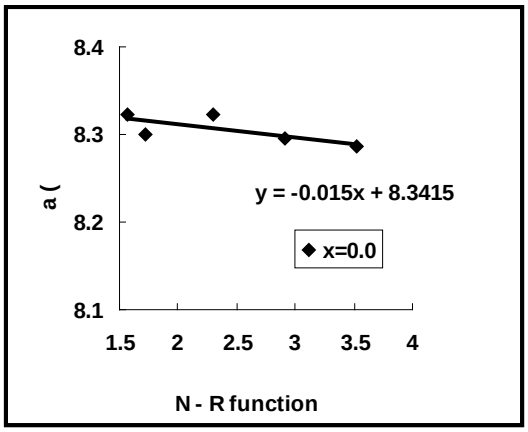

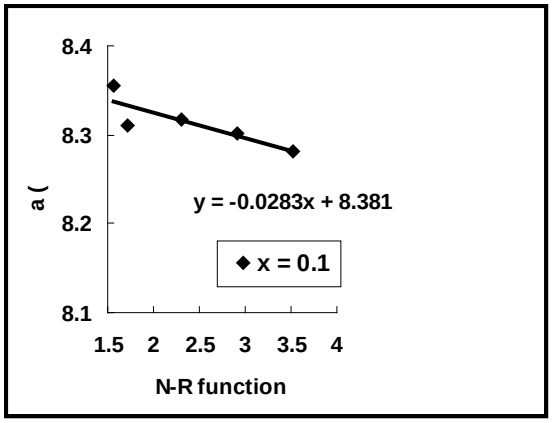

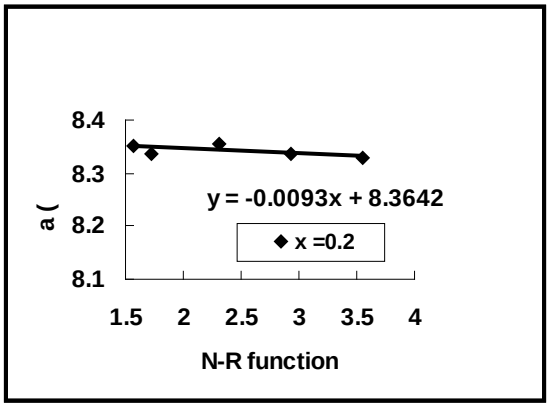

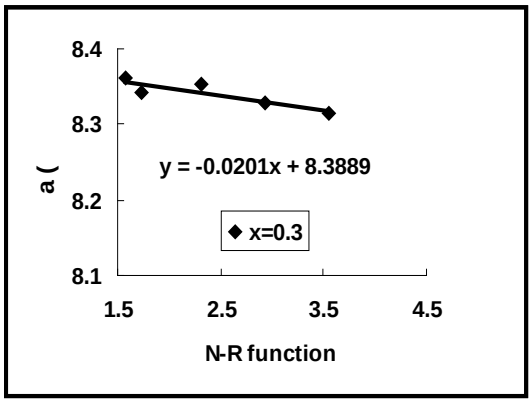

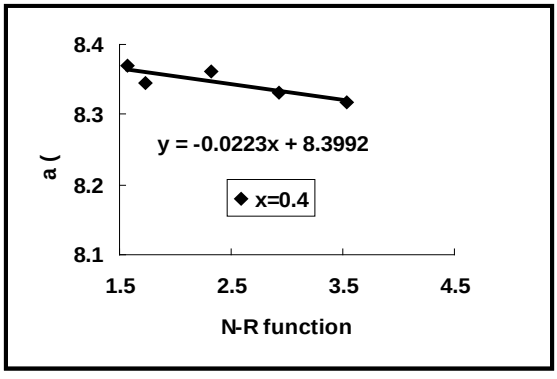

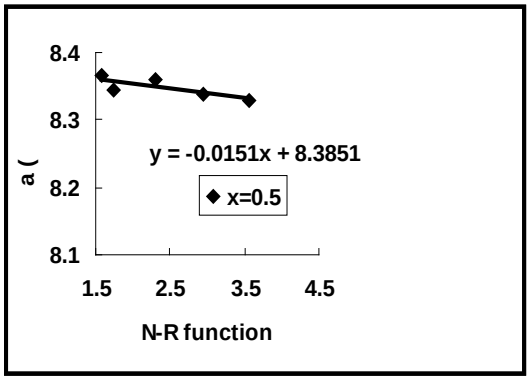

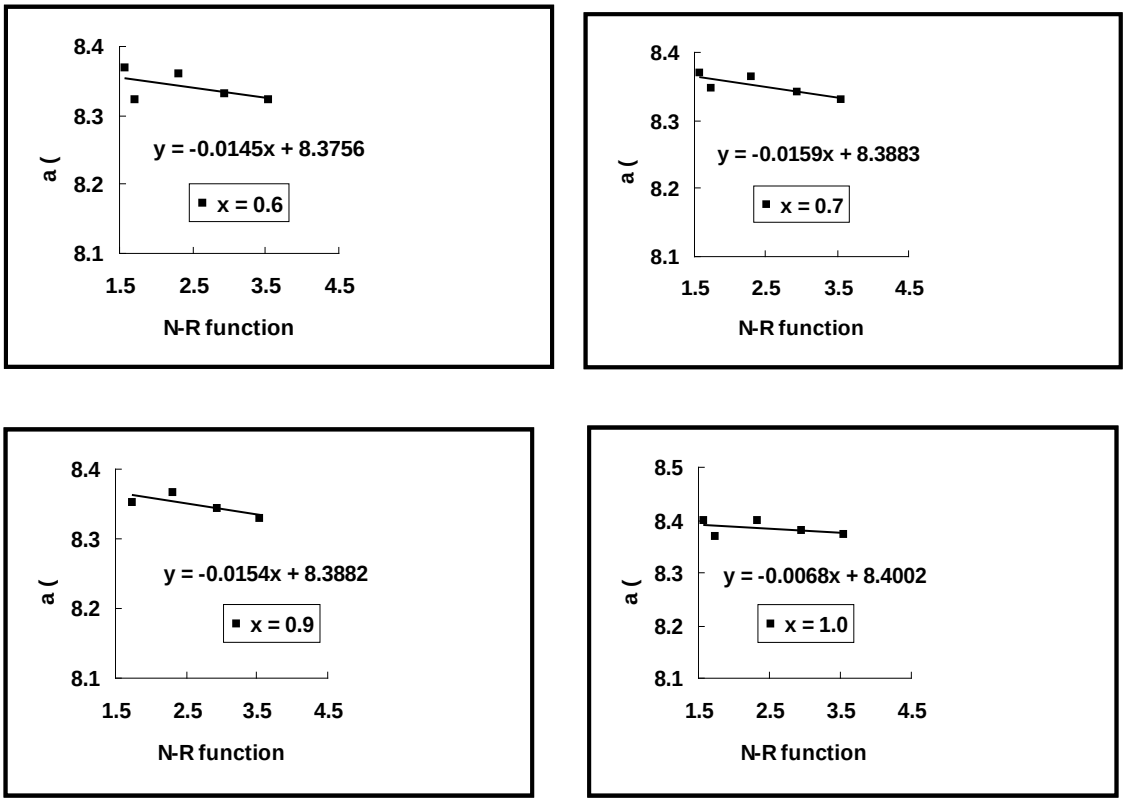

Fig. 5.10. Variation of the lattice parameters, a, in • , with N-R function for $Li_{0.5-x/2}Cu_xFe_{2.5-x/2}O_4$ sintered at 1100°C

Plot of N-R function in the sintering of 1200^{o}C

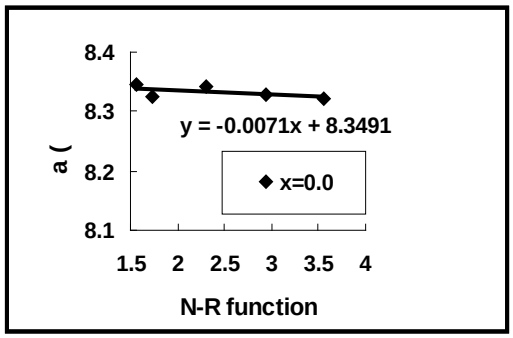

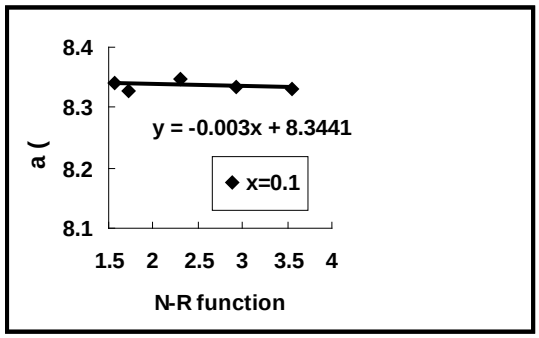

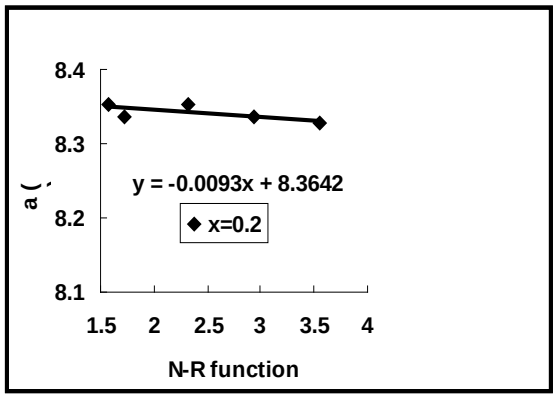

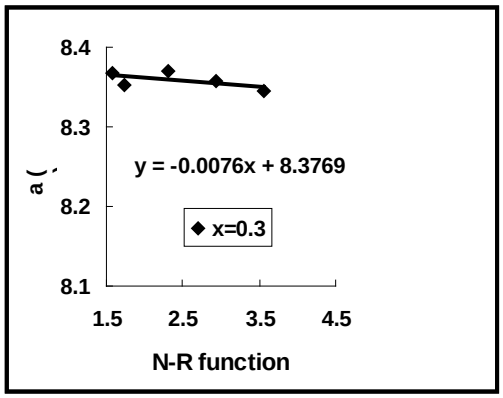

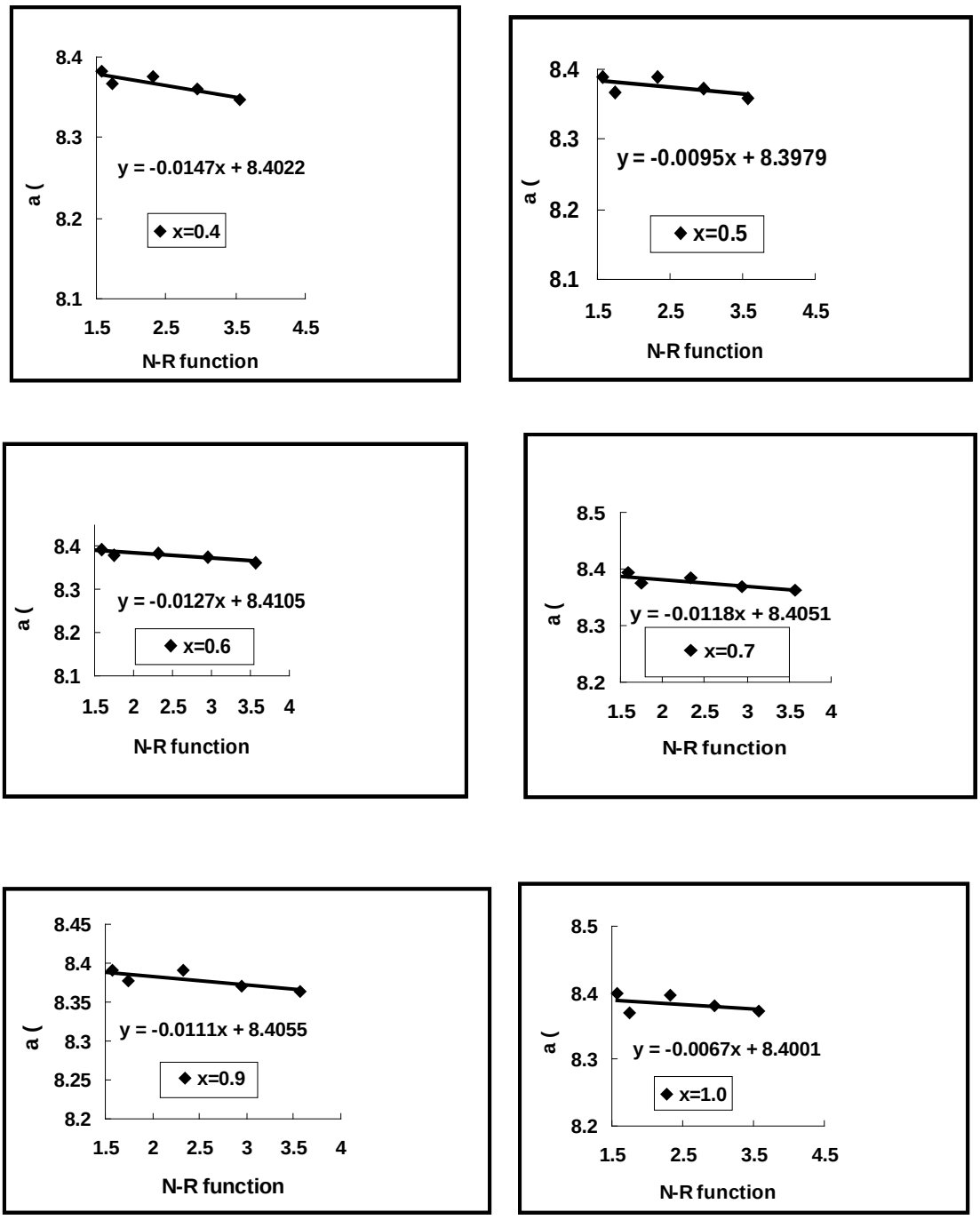

Fig. 5.11. Variation of the lattice parameters, a, in • , with N-R function for $Li_{0.5-x/2}Cu_xFe_{2.5-x/2}O_4$ sintered at 1200°C

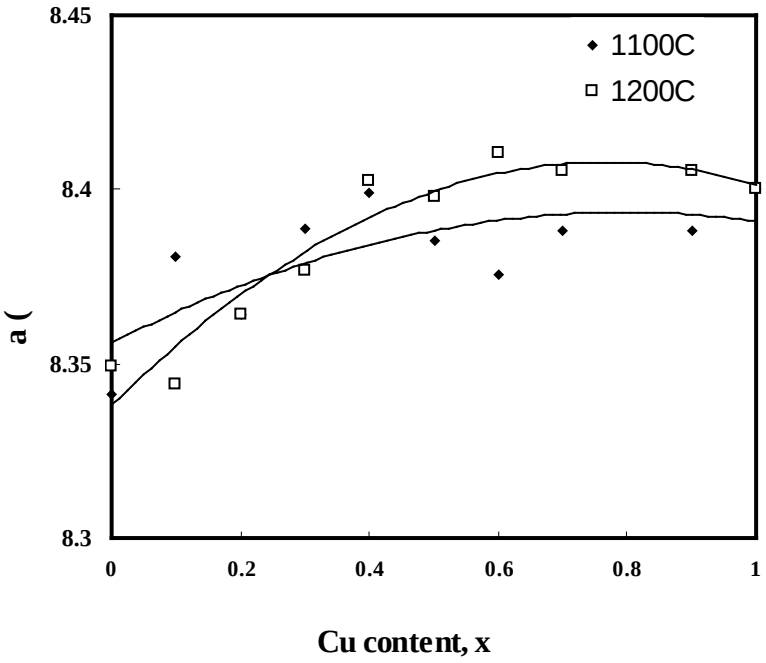

Fig. 5.12. Variation of the experimental lattice parameters 'a' with Cu content sintered at 1100°C and 1200°C respectively for $Li_{0.5-x/2}Cu_xFe_{2.5-x/2}O_4$ ferrites

Table 5.1: Lattice parameter, X-ray density, bulk density and porosity for the $Li_{0.5-x/2}Cu_xFe_{2.5-x/2}O_4$ where 0 • x • 1.

Cu content x	a(•) Sintered at 1200^0C	a(•) Sintered at 1100^0C	$\rho_{x\text{-ray}}$ (g/cc)	ρ_B (g/cc)	%P
0.0	8.349	8.341	4.72	3.48	26.06
0.1	8.344	8.381	4.81	3.78	21.36
0.2	8.364	8.364	4.84	3.87	19.96
0.3	8.376	8.388	4.90	3.95	19.34
0.4	8.402	8.399	4.92	4.07	17.21
0.5	8.397	8.385	5.00	4.15	16.93
0.6	8.410	8.375	5.05	4.24	15.87
0.7	8.405	8.388	5.13	4.33	15.55
0.9	8.405	8.388	5.28	4.85	8.02
1.0	8.402	8.402	5.36	4.95	7.58

Fig.5.13 shows the variation of x-ray and bulk densities as a function of Cu content of the samples. It is clearly shown that both densities increase with increasing Cu content. This can be ascribed to the atomic weight and density of Cu^{2+} (63.55, 8.94 g/cm^3, respectively) which are higher than that of Li^+ (6.94, 0.53 g/cm^3,) and Fe^{3+} (55.85, 7.87 g/ cm^3) [3] . At higher sintering temperatures grains formed uniformly and voids reduced and as a result the density is

increased. Porosity decreases with the increase of Cu content as shown in Fig. 5.14, which might be due to the effect of sintering temperature which provides more densification for the samples containing higher percentage of Cu.

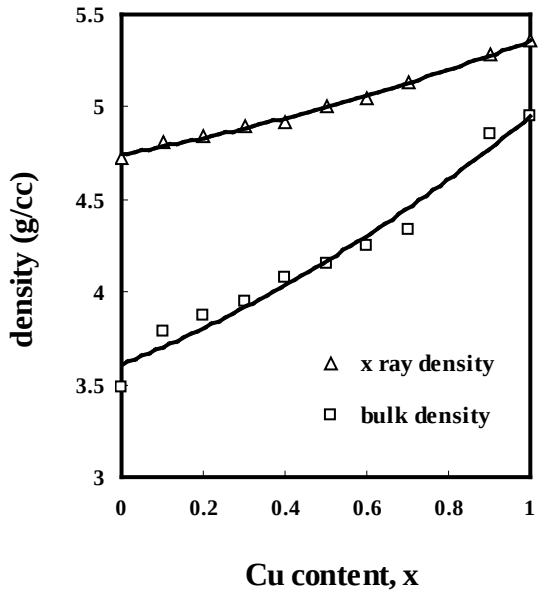

Fig. 5.13. Variation of X-ray and bulk densities with Cu content, x, for the samples $Li_{0.5-x/2}Cu_xFe_{2.5-x/2}O_4$, sintered at 1100^oC

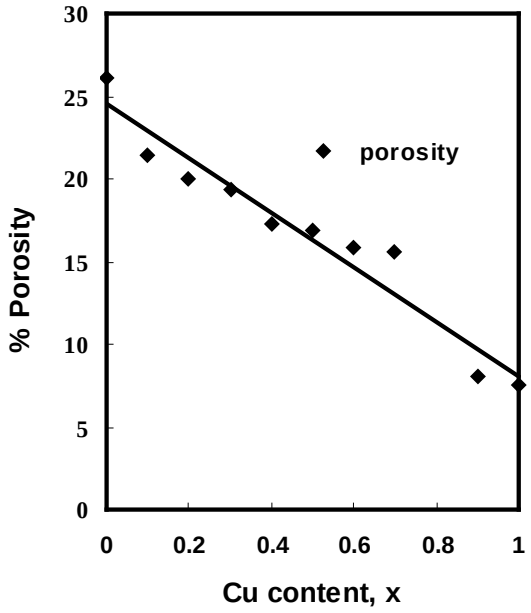

Fig. 5.14. Variation of % Porosity with Cu content, x, for the samples $Li_{0.5-x/2}Cu_xFe_{2.5-x/2}O_4$, sintered at 1100^oC

5. 2 The Study of Microstructure:

SEM microstructures for samples of composition up to x = 1.0 have been presented in Fig.5.15. The driving force for grain growth is the surface tension of the grain boundary [4]. Considering the distribution of grains on the surface of a polished section in Fig 5.15,.it can be observed that as in a foam, grains meet in groups of three at points and that the angle between the boundaries at these points is required by surface energy to be about 120^o. Because grains have various numbers of sides, it is necessary that most of the grain boundaries be curved. Grains having six sides can have straight boundaries and meet the requirement that adjacent boundaries form 120$^{o.}$. Grains having fewer than six sides will have boundaries which are concave when observed outward from the center of the grain. Most of the boundaries of grain having more than six sides will be convex when observed outward from the center of the grain. To decrease their total area, boundaries will move toward their centers of curvature. Thus grains having more than six sides will grow larger, and grains having less than six sides will grow smaller. These are the phenomenon of continuous grain growth where the size of all the grains is approximately equal. These conditions for continuous grain growth prevails up to x =

0.6. Beyond this composition grain size is not seen accurately, it might have exaggerated grain growth due to secondary recrystallization. When many pores are present and the sintering temperature is not too high for certain compositions, grain growth is inhibited. As a result, many pores become isolated from grain boundaries and diffusion distance between pores and grain boundaries become large. The average grain size was calculated by the linear intercept method. Grain size usually increases with the increasing of Cu content as shown in Table 5.2

Table 5.2: Average grain size, D_g for $Li_{0.5-x/2}Cu_xFe_{2.5-x/2}O_4$ sintered at 1100^{o}C

Cu content, x	D_g (μm)
0.0	4.04
0.1	6.04
0.4	11.35
0.6	24.12

← 50 μm →

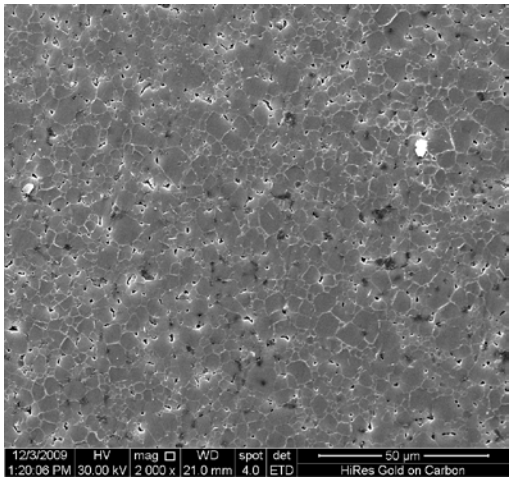

x = 0.0

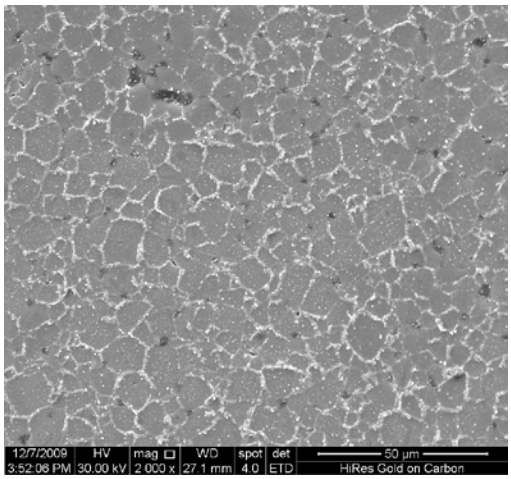

x = 0.1

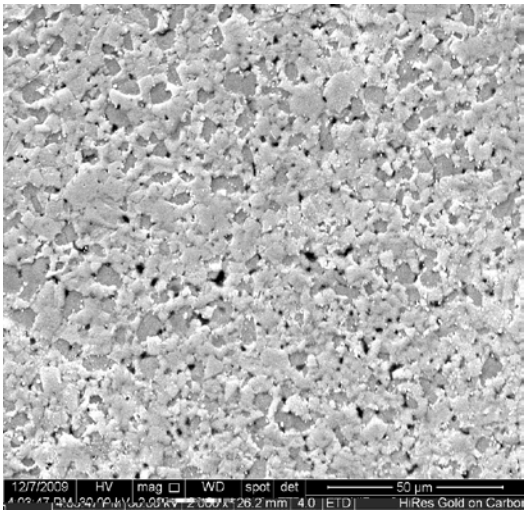

x = 0.2

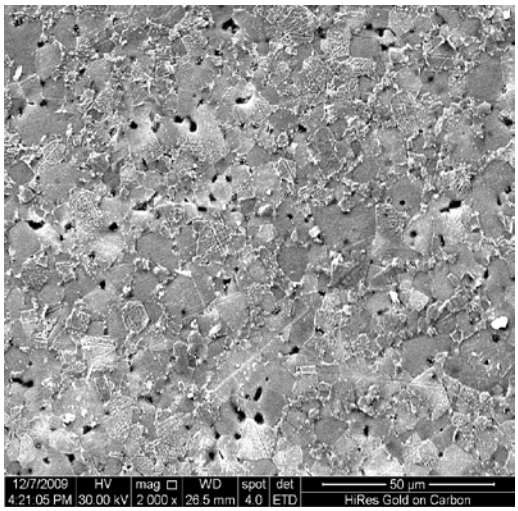

x = 0.3

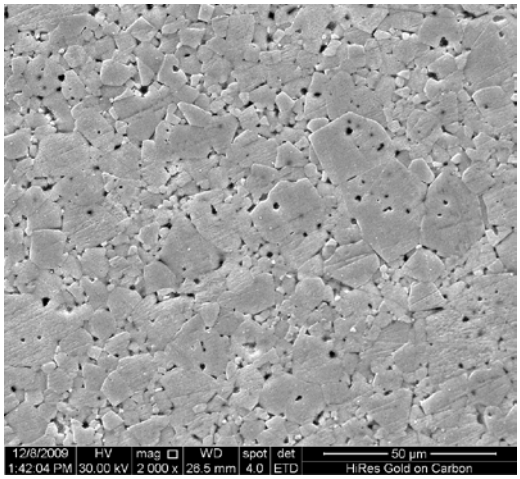

x = 0.4

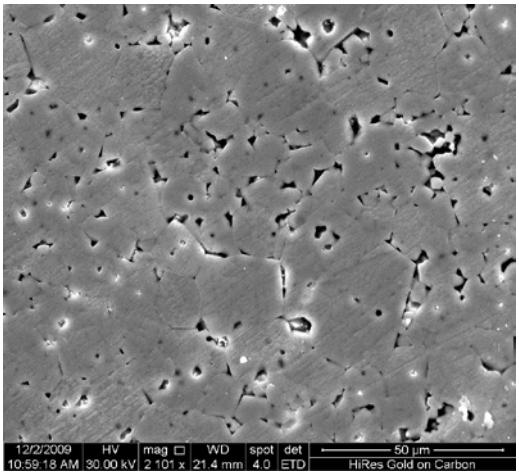

x = 0.6

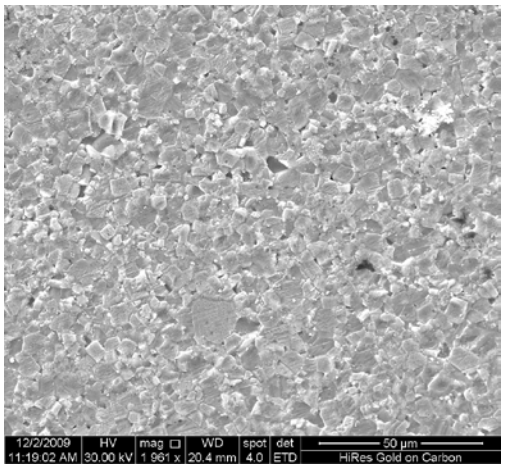

x = 0.8

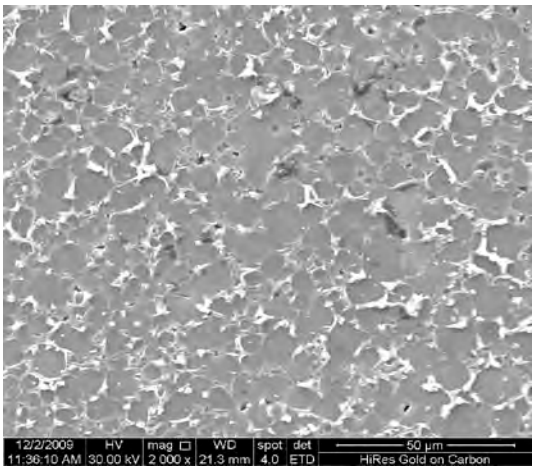

x = 1.0

Fig: 5.15. The microstructures of $Li_{0.5-x/2}Cu_xFe_{2.5-x/2}O_4$ samples sintered at 1100^oC

5.3 Measurement of Saturation Magnetization at room temperature

The magnetic moment for A and B sites μ_A and μ_B respectively and the net magnetic moment μ_m is given by

$$\mu_m = \mu_B - \mu_A \qquad (5.\ 3.1)$$

The relation between magnetization M and magnetic field H of $Li_{0.5-\ x/2}Cu_xFe_{2.5-x/2}O_4$, was studied at room temperature 298 K. The obtained results are shown in Fig 5.16 for different compositions. In Fig 5.17 is shown the variation of saturation magnetization M_s, with Cu composition x. It can be seen that the magnetization decreases with increasing Cu concentration. This behaviour can be explained by Néel's theorem of ferrimagnetism [5]. The individual magnetizations of the two sublattices, M_A and M_B cannot be observed but instead the net magnetization has been measured. Because the two magnetizations are oppositely directed, then

$$M = M_B - M_A \qquad (5.3.2)$$

This magnetization is proportional to the theoretical magnetic moments, which were calculated according to equation (5.3.1). Thus the variation of magnetic moment with Cu content could be explained by assuming that, as the concentration of Cu^{2+} ions increases, the relative number of Fe^{3+} ions decreases on both A and B sites, but the decrease on the B-sites is larger than that on the A sites. This will cause the A-B interactions to be reduced. According to Néel's molecular field model, the A-B exchange interaction is stronger than that of A-A or B-B. This decrease of A-B interaction was observed as the decrease of saturation magnetization with the increase of Cu^{2+} ions. The Bohr magneton of $Li_{0.5-x/2}Cu_xFe_{2.5-x/2}O_4$ calculated by relation

$$\mathbf{n_B = M M_s / 5585} \qquad (5.3.3)$$

where M is the molecular weight of the sample and M_S the saturation magnetization. It is observed that n_B decreases with increase of Cu content due to the decrease in resultant sublattices magnetic moment, as shown in Fig.5.18 and that are presented in Table 5.3.

Table 5.3 : Theoretical magnetic moment of $Li_{0.5-x/2}Cu_xFe_{2.5-x/2}O_4$

Cu content x	$Li_{0.5-x/2}Cu_xFe_{2.5-x/2}O_4$	Theoretical magnetic moment $(\mu_B)_{th}$	Experimental magnetic moment $(\mu_B)_{exp}$
0.0	$Li_{0.5}Fe_{2.5}O_4$	2.50	3.01
0.1	$Li_{0.45}Cu_{0.1}Fe_{2.45}O_4$	2.35	2.54
0.3	$Li_{0.35}Cu_{0.3}Fe_{2.35}O_4$	2.05	2.43
0.4	$Li_{0.30}Cu_{0.4}Fe_{2.30}O_4$	1. 90	2.29
0.5	$Li_{0.25}Cu_{0.5}Fe_{2.25}O_4$	1.75	2.04
0.6	$Li_{0.20}Cu_{0..6}Fe_{2.20}O_4$	1.60	1.79
0.7	$Li_{0.15}Cu_{0..7}Fe_{2.15}O_4$	1.45	1.67
0.9	$Li_{0.05}Cu_{0.9}Fe_{2.05}O_4$	1.15	1.33
1.0	$CuFe_2O_4$	1.00	1.19

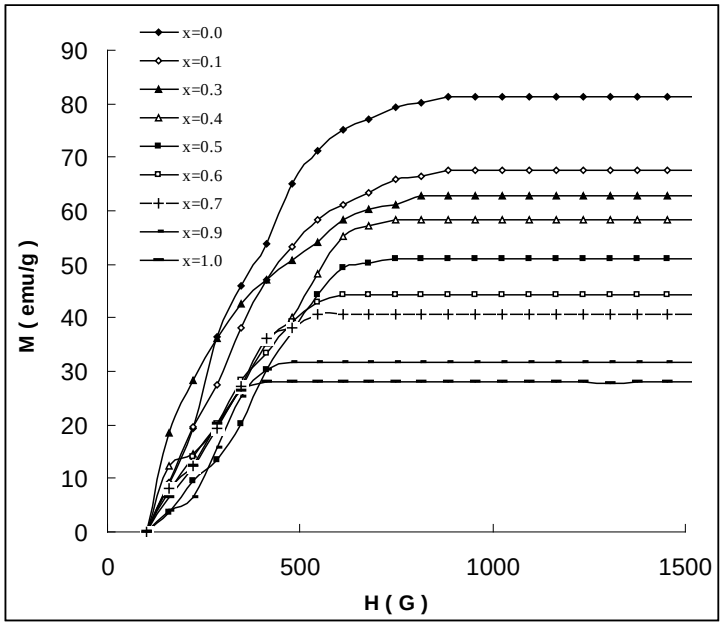

Fig. 5.16. The magnetization (M) versus the applied magnetic field (H) curves at room temperature for $Li_{0.5-x/2}Cu_xFe_{2.5-x/2}O_4$ sintered at 1100^oC

.

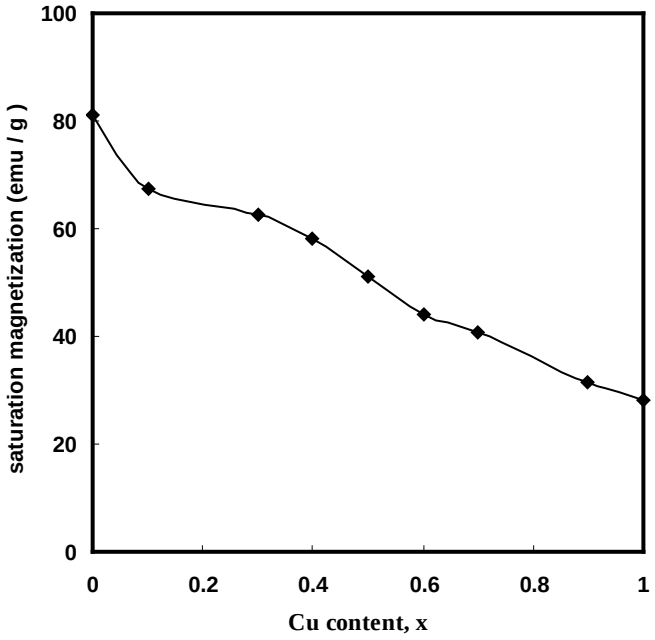

Fig. 5.17. Variation of saturation magnetization, M_s, with Cu composition, x, for $Li_{0.5-x/2}Cu_xFe_{2.5-x/2}O_4$ sintered at 1100^oC at room temperature**.**

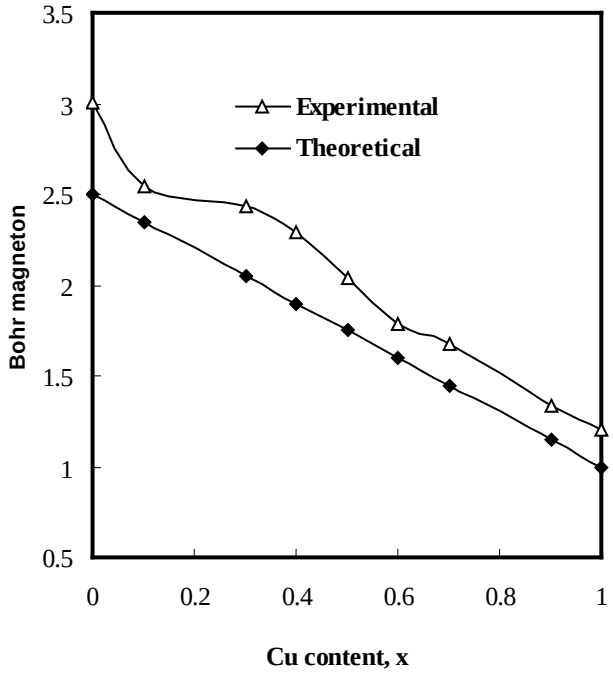

Fig . 5.18. Variation of magnetic moment as a function Cu content , x , for $Li_{0.5-x/2}Cu_xFe_{2.5-x/2}O_4$ sintered at 1100°C at room temperature

.

5.4 Curie Temperature (T_C) Measurement

Curie temperature is a measure of exchange force in ferrimagnetism. It is the temperature at which the thermal energy tends to disorder the system to win over the exchange energy tending to order the system magnetically. At this temperature, ferrimagnetic substance changes over to a paramagnetic substance. The temperature dependence of the initial permeability for the toroid shaped ferrite samples are presented in Fig 5.19 and 5.20 for the sintering temperature of 1100°C and 1200°C, respectively. Permeability falls rapidly when the magnetic state of the ferrite samples changes from ferrimagnetic to paramagnetic. The sharp falling of μ_i' with temperature shows the degree of homogeneity [6- 7] for samples. The initial permeability falls abruptly close to the Curie temperature, T_C. From the curves of the initial permeability μ_i verses temperature, it can be seen that for samples with x = 0, μ_i increases gradually until it attains a maximum value near T_C while for the other samples such as x = 0.1 to 1, a second broadening peak is found before at T_C. This could be explained by the change

cubic to tetragonal deformation with the inclusion of Cu ions . It has been mentioned earlier that though tetragonal deformation is not perceptible from X-ray diffraction patterns, it exists due to Jahn-Teller deformation of Cu^{2+} ions.

Fig 5.21 represents the variation of T_C as a function Cu content, x at different sintering temperatures of 1100^{o}C and 1200^{o}C respectively. It is observed that T_C decreases with the increase of Cu contents due super-exchange interaction between A and B sites weaken. Curie temperature decreases linearly up to x = 0.5 and x = 0.7 for the sintering temperatures of 1100^{o}C and 1200^{o}C, respectively. It is seen that the linearity of T_C vs Cu content increases for the sintering temperature of 1200^{o}C than the sintering temperature of 1100^{o}C. It is due to the fact that for the higher sintering temperature tetragonal deformation decreases. For the sintering temperature 1100^{o}C, the values of Curie temperature for $Li_{0.5}Fe_{2.5}O_4$ and $CuFeO_4$ were found to be 675^{o}C and 425^{o}C, respectively while for the sintering temperature of 1200^{o}C, the Curie temperatures were found as 650^{o}C and 365^{o}C, respectively. The Curie temperatures given in the literature are 670^{o}C and 455^{o}C for Li ferrite and Cu ferrite respectively [8]. It can be observed that the deviation of Curie temperature for the samples are more for higher Cu content due to more tetragonal distortion. The more the sintering temperature increases the more the structure changes from tetragonal to cubic structure.

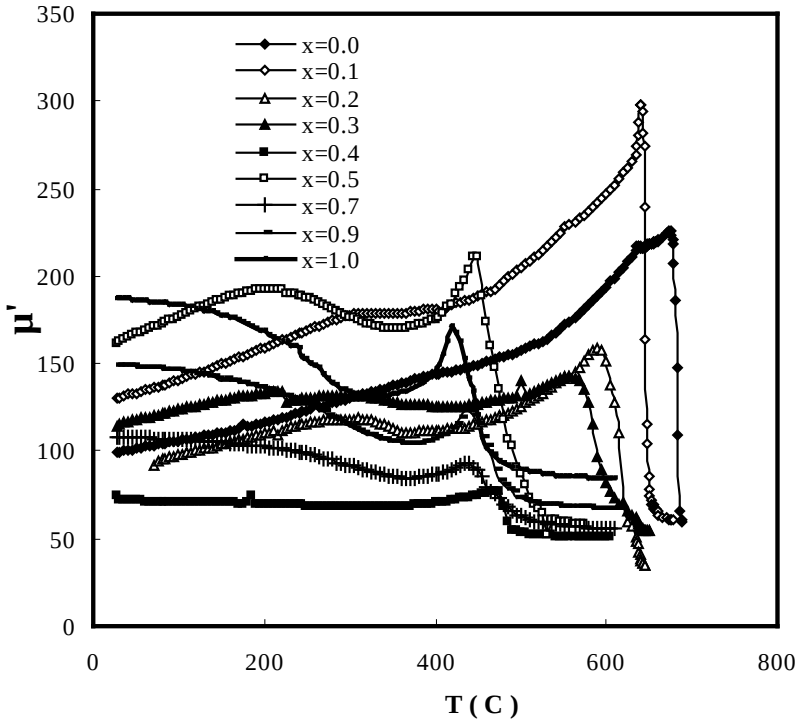

Fig. 5.19. Variation of initial permeability μ_i' with temperature T in ^oC for $Li_{0.5-x/2}Cu_xFe_{2.5-x/2}O_4$ in the sintering temperature of $T_S = 1100^oC$

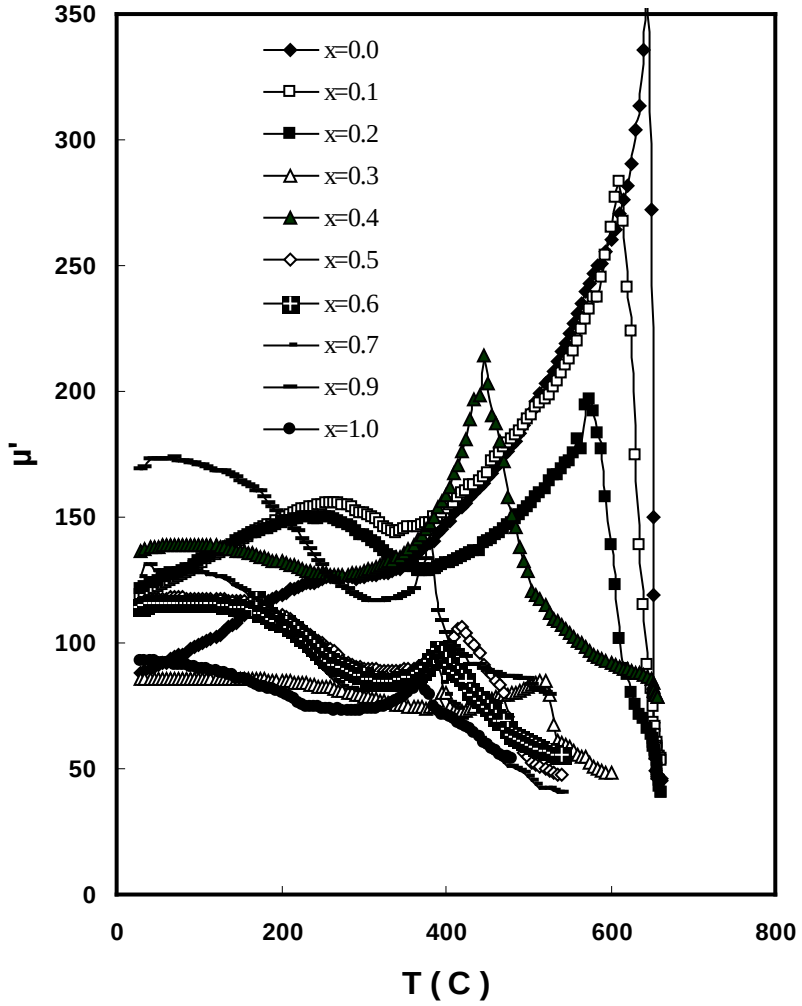

Fig. 5.20. Variation of initial permeability μ_i' with temperature T in ^oC for $Li_{0.5-x/2}Cu_xFe_{2.5-x/2}O_4$ in the sintering temperature of $T_S = 1200^oC$

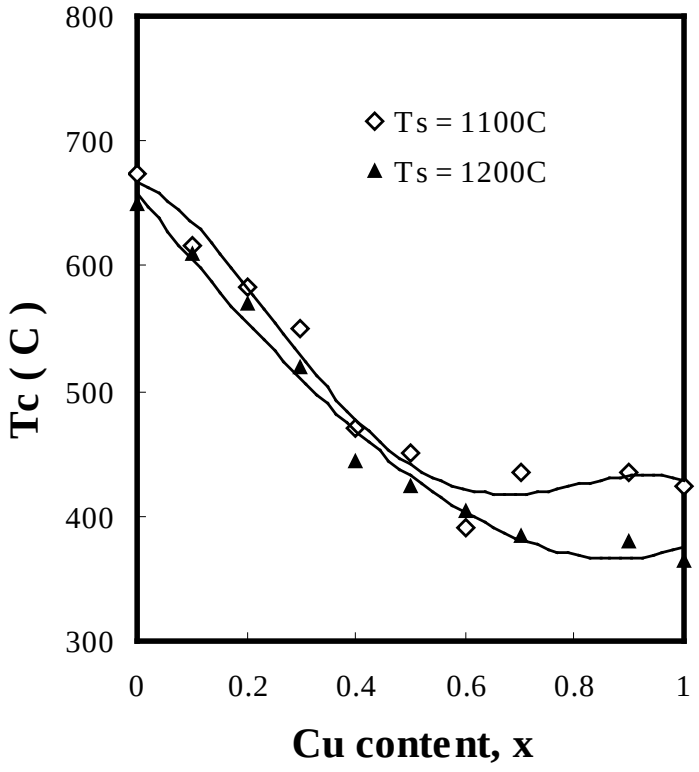

Fig. 5.21. Variation of T_C with respect to Cu content, x, in the sintering temperature of 1100^0C and 1200^0C for $Li_{0.5-x/2}Cu_xFe_{2.5-x/2}O_4$

5.5 Complex Permeability

The complex permeability is given by $\mu^* = \mu' - i\mu''$, where μ' and μ'' are the real and imaginary parts of initial permeability, respectively. The real part μ' describes the stored energy expressing the component of magnetic induction ***B*** in phase with the alternating magnetic field ***H.*** The imaginary part μ'' describes the dissipation of energy expressing the component of magnetic induction ***B*** out of phase with the alternating magnetic field ***H.***

The permeability can be expressed as $\mu = 1+ \bullet_{spin} + \bullet_{dw}$, where $\bullet_{spin}$ is the susceptibility due to spin and $\bullet_{dw}$ is the susceptibility due to domain wall motion. The dispersion of domain wall component depends on the square of the frequency and that of the spin rotational component is inversely proportional to the frequency. The domain wall motion contribution starts to decrease at lower frequency and the spin rotational component decreases at relatively higher frequencies. Globus [9] et al have developed an equation correlating static susceptibility (μ_s-1), resonance frequency f_r, saturation magnetization M_s and grain diameter, D as given below:

$$(\mu_s\text{-}1) = (3M_s^2 \quad 4\bullet D) \quad /16 \quad E_w \qquad (5.5.1)$$

$$f_r = (16 \quad E_w) \quad / \quad \bullet\bullet D^2 \qquad (5.5.2)$$

where E_w is the wall energy given by $E_w = K\bullet w$, here K is the anisotropic energy and $\bullet w$ is the domain wall thickness.

$$(\mu_s\text{-}1) = (12 \quad M_s^2 \quad) \quad / \quad \bullet D^2 \qquad (5.5.3)$$

where $\bullet$ is the domain wall domain damping factor.

According to this model, the larger grain size leads to high permeability and low resonance frequency. The smaller grain size leads to higher resonance frequency. In our experiment, we would apply Globus model in which the permeability is directly proportional to the microstructural features. i.e grain size. As grain size increases, the multi domain grains are obtained which induces in higher permeability values due to the domain wall contribution.

Thus , the domain wall motion is affected by the grain size and enhances with the increase of grain size. Also an increase in the density of the Cu contents not only results in the reduction of demagnetizing field due to reduction of pores but also rises the spin rotational contribution, which in turn increases permeability.

In Fig 5.22, the real part of the complex initial permeability μ_i up to f = 13 MHz have been presented for different composition in the range $0 \leq x \leq 1$, sintered at 1100 ^{o}C. The general characteristics of the curves in Fig. 5.22 is that μ' remains fairly constant in the frequency range shown in the figure up to some critical frequency characterized by the onset of resonance. At these frequencies, after a small rise, the curves drop fairly rapidly to a very small value. This phenomenon is called ferrimagnetic resonance [10]. This trend of the curve is clearly visible for higher Cu content. The resonance frequency peaks are the result of the absorption of energy due to the matching of the oscillation frequency of the magnetic dipoles and the applied frequency. The initial permeability of $CuFe_2O_4$ is highest than other composition. This is because the sintered density is highest and the porosity is lowest for this composition. This shows that the high permeability ferrite can be used in high quality coils as a core only in a limited frequency range. The variation of imaginary part of initial permeability μ'' with frequency for samples of different compositions is shown in Fig. 5.23. It is observed that the rise in permeability with the increase of Cu content is associated with the rise in loss represented by μ'' .The addition of Cu lowers the anisotropy constant and reduces the natural frequency of precession, which leads to the onset of resonance at lower frequency

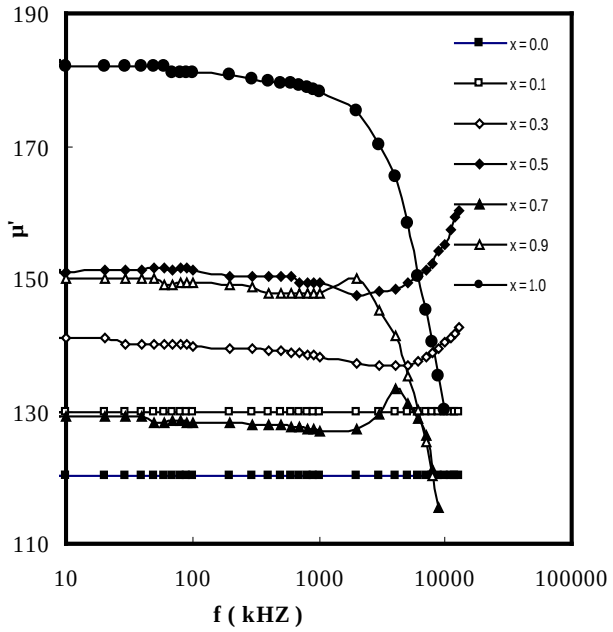

Fig 5.22 Variation of the real part of the initial permeability with frequency for $Li_{0.5-x/2}Cu_xFe_{2.5-x/2}O_4$ samples.

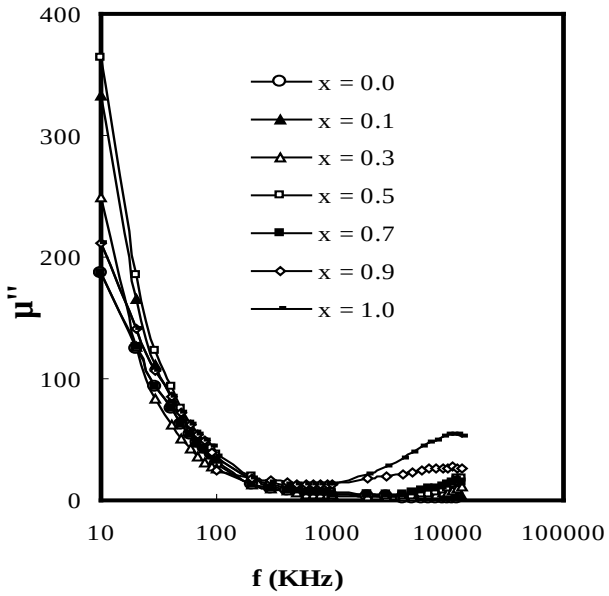

Fig. 5.23. Variation of the imaginary part of the initial permeability with frequency for $Li_{0.5-x/2}Cu_xFe_{2.5-x/2}O_4$ samples.

5.6 Coercivity and hysteresis loss

In materials science, the coercivity also called the coercive field of a magnetic material is the intensity of the applied magnetic field required to reduce the magnetization of that material to zero after the magnetization of the sample has been driven to saturation. Coercivity is usually measured in oersted or ampere/meter units and is denoted $H_{C.}$

The B-H loops were measured for the Li-Cu ferrite for the sintering temperature of $1200^{o}C$ at constant frequency f = 1200 Hz and room temperature and has been presented in Fig. 5.24. The hysteresis curve and its properties such as the retentivity, coercivity and hysteresis loss are very useful information from application point of view. In Fig. 5.25 and 5.26 both indicate the hysteresis loss and coercivity, respectively as a function of composition. The decrease of loss with increasing of Cu content is due to the fact that the decrease of intrinsic magnetization. The increase the area within the loop near the lower Cu content end side. This leads to the lower value of hysteresis loss with the increase of Cu content. Coercivity and hysteresis loss decrease with the increase of Cu content due to increased magnetic softness at the Cu-rich end.

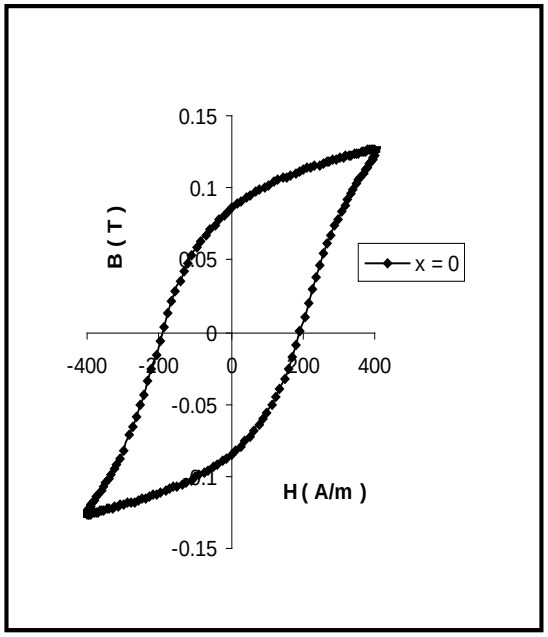
0.15
0.1
0.05
0
-0.05
-0.1
-0.15
-400
-200
0
200
400
B (T)
H (A/m)
x = 0

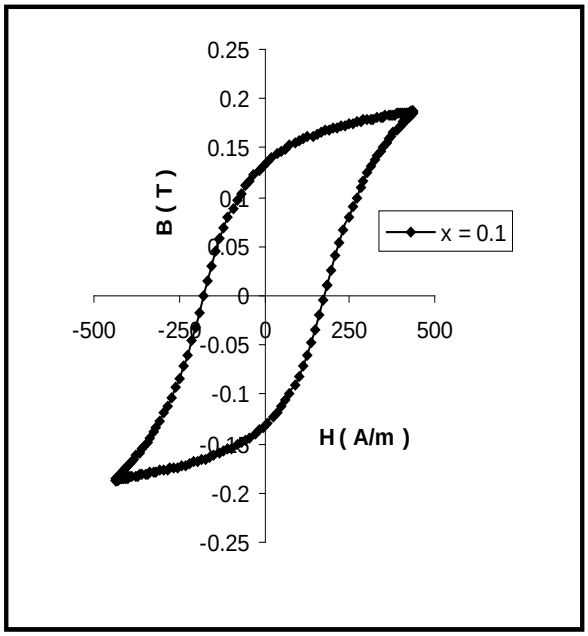
0.25
0.2
0.15
0.1
0.05
0
-0.05
-0.1
-0.2
-0.25
-500
-250
0
250
500
B (T)
H (A/m)
x = 0.1

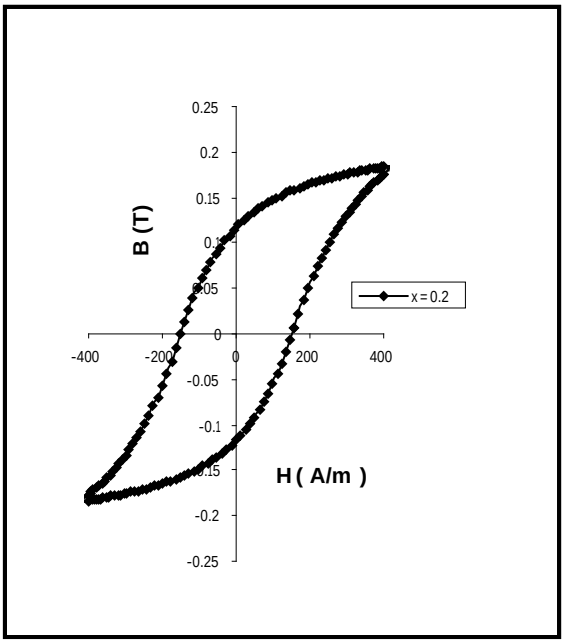
0.25
0.2
0.15
0.05
0
-0.05
-0.1
-0.2
-0.25
-400
-200
0
200
400
B (T)
H (A/m)
x = 0.2

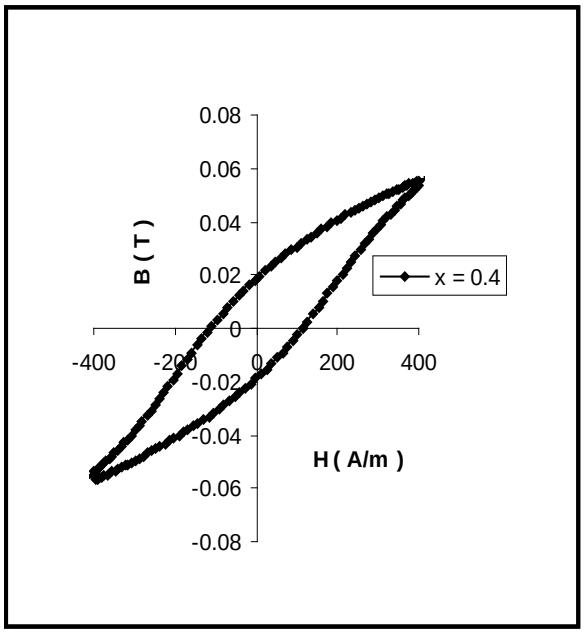
0.08
0.06
0.04
0.02
0
-0.02
-0.04
-0.06
-0.08
-400
-200
0
200
400
B (T)
H (A/m)
x = 0.4

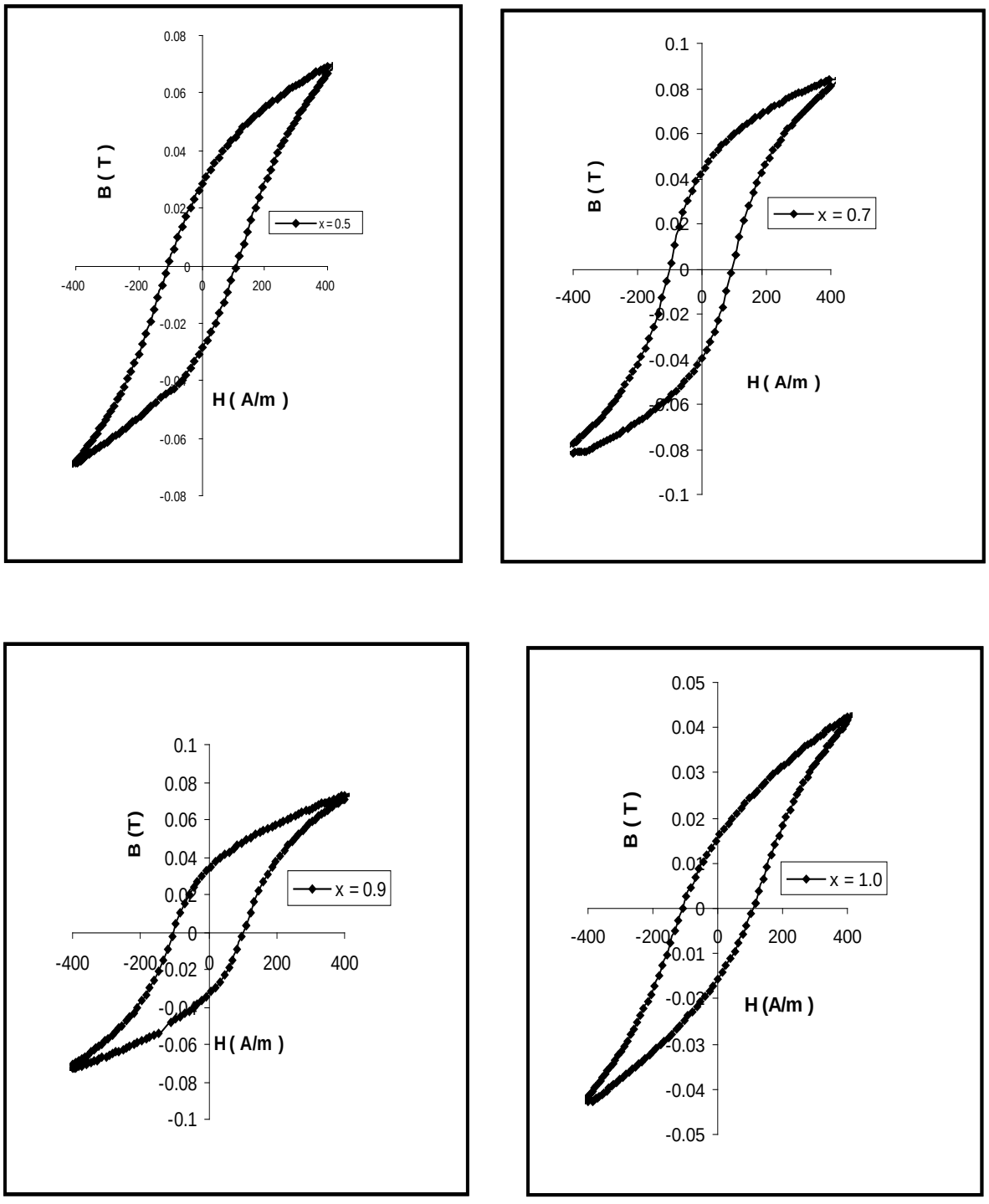

Fig. 5.24. B-H loops for $Li_{0.5-x/2}Cu_xFe_{2.5-x/2}O_4$ samples

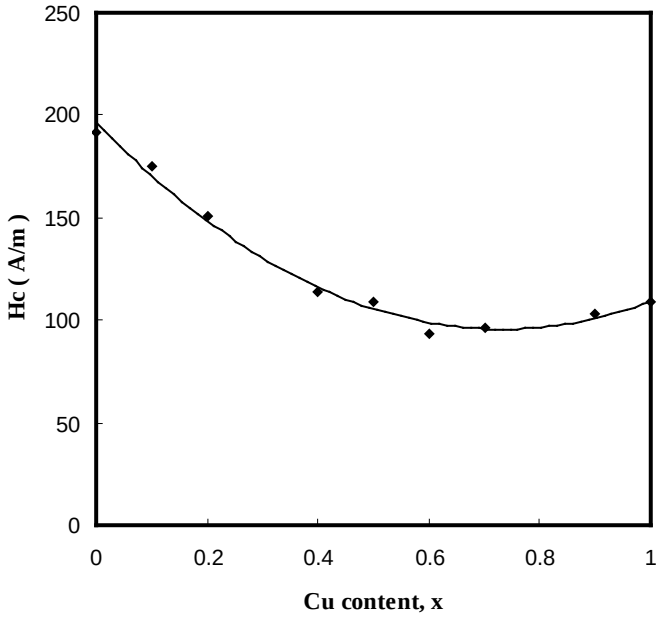

Fig. 5.25. Variation of H_C with Cu content, x for $Li_{0.5-x/2}Cu_xFe_{2.5-x/2}O_4$ samples

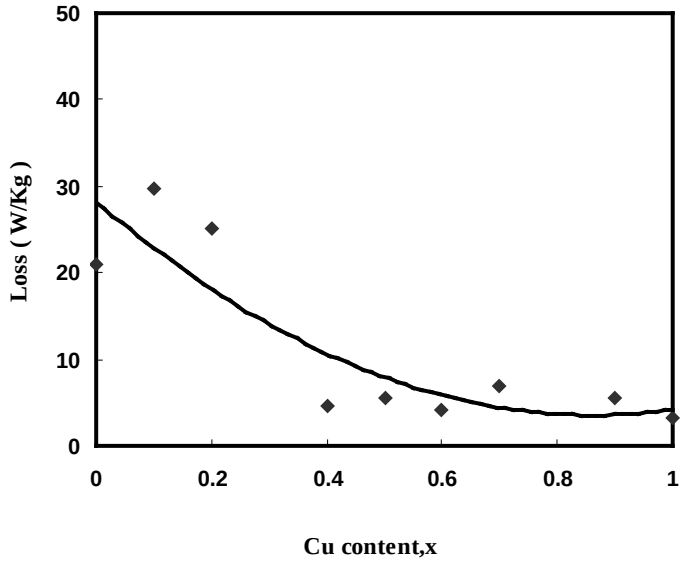

Fig. 5.26.Variation of hysteresis loss with Cu content, x for $Li_{0.5-x/2}Cu_xFe_{2.5-x/2}O_4$ samples

5.7 Electrical Resistivity and Activation Energy :

Fig. 5.27 shows the variation of the electrical resistivity, log(•) with 1000/T for the investigated of $Li_{0.5-x/2}\ Cu_xFe_{2.5-x/2}O_4$ samples. It is obvious that the electrical resistivity decreases with increasing temperatures, illustrates that all samples exhibit semiconducting behaviour as usual ferrites characteristics. The most probable conduction mechanism is electron hopping between Fe^{2+} and Fe^{3+} ions : Fe^{2+} • $Fe^{3+} + e^-$ (n-type). This process is expected to take place between two adjacent octahedral sites in the spinel lattice. This is due to the fact that at high temperature, the thermal energy is sufficiently great to create vacancies and the activation energies represent a sum of the energies required for vacancies generation and the motion of the electrons into the vacancies. Activation energy (E_a) has been estimated for different composition, x and presented in Table 5.4. It is observed that activation energy is higher for higher Cu content. This is because with the increase of Cu content ferromagnetic ordering weakens. It requires more energy for electronic conduction to occur in the more magnetically disordered state.

In Fig 5.28, • is shown as a function of composition, x at room temperature. The highest value of • is obtained for x = 0.3. For x > 0.3, resistivity decreases with the increase of Cu composition x. When polycrystalline ferrites are considered, the bulk resistivity arises from a combination of crystalline resistivity and the resistivity of the crystalline boundaries. The boundary resistivity is much greater than that of crystalline resistivity so the boundaries have the greatest influence on d.c. resistivity. The decrease of resistivity is also related to the decrease of porosity since pores are non-conductive, which increases the resistivity of the material. The resistivity decreases with decreasing of porosity, because the charge carriers on their way face the pores. The IR spectrum of $Li_{0.5-x/2}Cu_xFe_{2.5-x/2}O_4$ ferrite by Mazen [11], for the sample with x = 0 to 0.1, shows a change in the absorption bands, some disappeared and some born, By introducing the divalent Cu^{+2} ions, for the tetrahedral site (A-site) all the subsidiary bands disappeared completely at x = 0.3, while the octahedral site (B-site) the band of divalent Fe^{+2} ion changed to small shoulder starting from x = 0.3. This indicate that Fe^{+2} ions are present as traces in the samples of x• 3. From these discussions, in Fig 5.26, at room

temperature, resistivity increases up to x = 0.3, but it decreases x > 0.3, which can be attributed Fe^{3+} and Li^{+} concentration are decreasing with increases of Cu^{+2} content, but Fe^{2+} ions are increased.

.

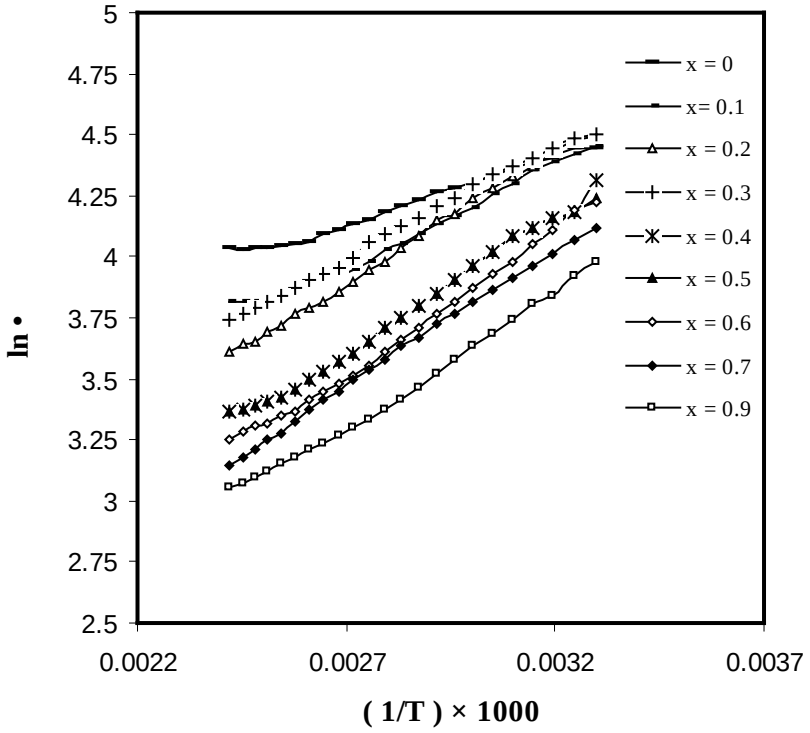

Fig 5.27 Variation of electrical resistivity ln • with temperature in 1000/T for $Li_{0.5-x/2}Cu_xFe_{2.5-x/2}O_4$ samples

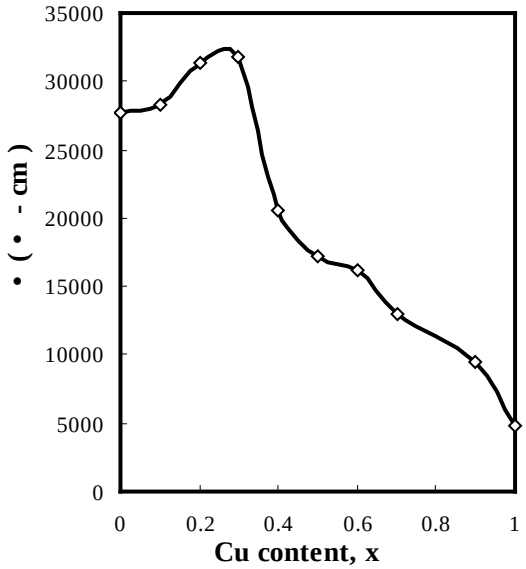

Fig. 5.28. Variation of electrical resistivity with Cu content at room temperature for $Li_{0.5-x/2}Cu_xFe_{2.5-x/2}O_4$ samples

Table 5. 4 : Activation energy and electrical resistivity at room temperature for $Li_{0.5-x/2}Cu_xFe_{2.5-x/2}O_4$ samples

Cu content, x	Activation Energy, E_a (eV)	Electrical resistivity, • (• -cm)
0.0	0.106	27765
0.1	0.157	28345
0.2	0.211	31304
0.3	0.182	31785
0.4	0.219	20563
0.5	0.214	17268
0.6	0.227	16821
0.7	0.221	12996
0.9	0.217	9446

5.8 Temperature dependence dielectric constant

The temperature variation of dielectric constant, •′ has been studied at 10 kHz and shown in Fig.5.29. It can be seen that the dielectric constant increases slowly with the temperature in

the beginning and after that increases rapidly and sharply for different samples. The resistivity of ferrites decreases with increase in temperature. According to Koops [12] the dielectric constant is inversely proportional to the square root of resistivity. Therefore, the increase in dielectric constant with temperature is expected.

The dielectric constant in ferrites is attributed to the four types of polarization, viz., interfacial, dipolar, ionic and electronic polarization. At low frequencies, dipolar and interfacial polarization, which are strongly temperature dependent, play the dominant role. Interfacial polarization is known to increase with the increase of temperature while the dipolar polarization decreases with the increase of temperature. The charge carriers in ferrites are not completely free but strongly localized. The increase in temperature thermally activates the charge carriers and their drift mobility. This increase the electronic exchange interaction thereby enhancing the dielectric constant. The present increase in the dielectric constant with increase in temperature may be indicative of the dominant role played by the interfacial polarization. The observed temperature dependence of dielectric constant can be explained with the help of relaxation time [13] and is given by $\bullet = \bullet_o \exp (E_a / kT)$, where E_a is the value of activation energy and k is the Boltzmann constant. According to Debye's equation, dielectric constant and relaxation time are inverse relation with each other. At low temperature, the value of relaxation time is high and hence dielectric constant is low. As the temperature is increased, thermal energy provided to the sample plays a role to decrease the relaxation time and hence there is an increase in dielectric constant.

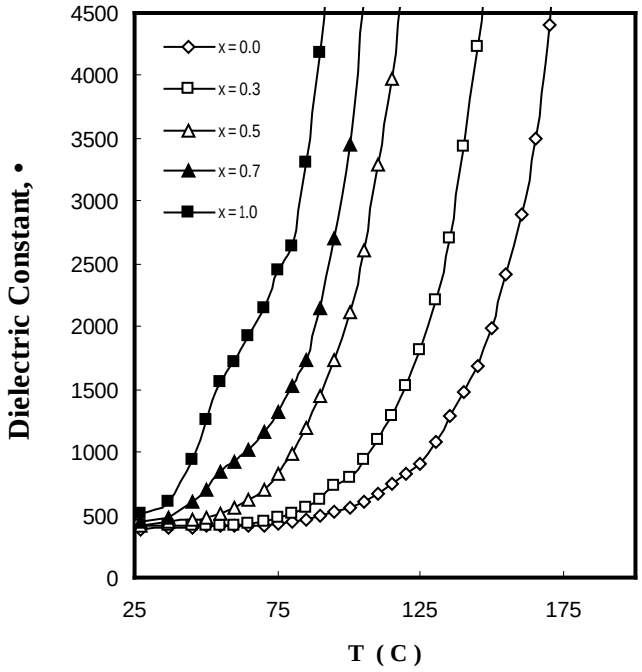

Fig. 5.29.Variation of dielectric constant • with temperature for $Li_{0.5-x/2}Cu_xFe_{2.5-x/2}O_4$

5.9 Frequency dependence dielectric constant

The variation of dielectric constant with frequency in the range of 10 kHz to 500 kHz at room temperature is shown in Fig. 5.30.This behavior of a dielectric may be explained qualitatively by the fact that the mechanism of the polarization process in ferrite is similar to that of the conduction process. The electron hopping (Fe^{2+} • Fe^{3+} or Cu^{2+} • Cu^{+}) occurs by electron transfer between adjacent octahedral sites (B-sites) in the spinel lattice [11]. Thus by the electronic exchange : Fe^{2+} + Cu^{2+} • Fe^{3+} + Cu^{+} one obtains local displacements of electrons in the direction of the applied field, these displacements determine the polarization of the ferrite. It is known that the effect of polarization is to reduce the field inside the medium. Hence, the dielectric constant is decreased as the frequency is increased.

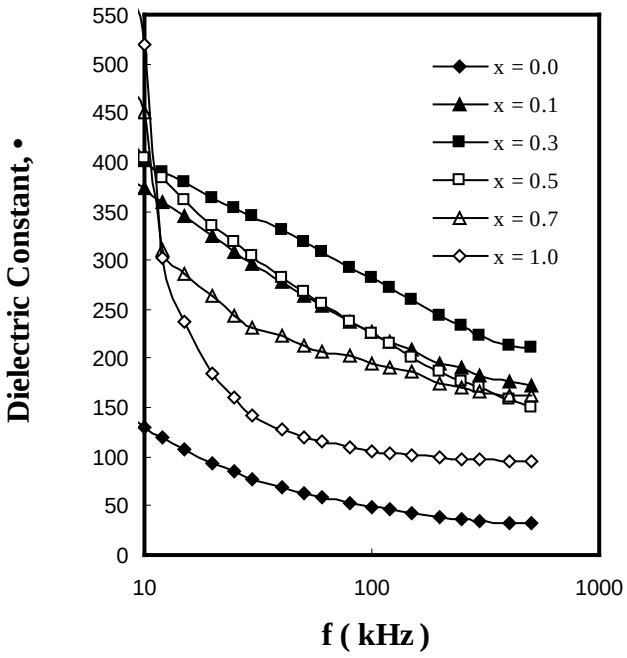

Fig.5.30. Variation of dielectric constant • with frequency for $Li_{0.5-x/2}Cu_xFe_{2.5-x/2}O_4$

References:

[1] S. A. Mazen and H. A. Dawoud , *Structure and Magnetic Properties of Li-Cu Ferrte*, phys. Stat. sol. (a) 172, 275 (1999)

[2] L. Vegard, Z. Phys., 5, 17 (1921)

[3] William D. Callister, An Introduction Materials Science and Engineering, John Wiley & Sons, Inc. (2001)

[4] R. L. Coble, J. E. Burke in J E Burke (Ed) *Sintering in ceramics, Progress in Ceramic Science* vol 3, p- 474

[5] K. J. Standly, *Oxide Magnetic Materials*, Clarendon Press, Oxford 1972

[6] E. Cedillo, J. Ocampo, V. Rivera and R. Valenzuela, "*An apparatus for the measurement of initial magnetic permeability as a function of temperature*", Journal of Physics F: Scientific Instrument, 13, 383 (1980)

[7] R. Valenzuela, "A sensitive method for the determination of the Curie temperature in ferrimagnets", Journal of Material Science, 15, 3137 (1980)

[8] J. Smith and H. P. J. WIJN, *Ferrites, Wiley, New York* 1959

[9] Glubus, A. and Duplex, P. " *Size of bloch wall and parameters of the magnetic susceptibility in ferromagnetic spinels and garnets*, Phys. Stat. Sol. A 31(1969) 765

[10] F. G. Brockman, P. H. Dowling, W. G. Steneck, Phys. Rev. 77 (1950) 85.

[11] S. A. Mazen *" Infrared absoption and dielectric properties of Li-Cu ferrite"* Mater, Chem. Phys.62 (2000) 139-147.

[12] A. M. Shaikh, S. S. Bellad, B. K. Chougule, *" Temperature and frequency dependent dielectric properties of Zn substituted Li-Mg ferrites"* J. Magn. Magn. Mater. 195, 384, (1999)

[13] M. Maisnam, S. Phanjoubam, H. N. K. Sarma, O. P. Thakur, L. Radhapiyari Devi and Chandra Prakash, "Influence of temperature on the dielectric behaviour of Co^{2+} substituted Li-Ni-Mn ferrites" Ind. J. Engg. Mat. Sci. 15, 199, (2008)

Chapter Six

Conclusions

A series of polycrystalline samples with the stoichiometric composition having the general formula $Li_{0.5-x/2}Cu_xFe_2O_4$, where x = 0 to 1, have been prepared using conventional double sintering ceramic method, sintered at 800°C 1000°C, 1100 °C, 1200 °C for 3 hours. The samples are characterized by X-ray diffraction which confirms the spinel structure. For the sintering temperature of 800°C, x = 0.9 and 1.0 both the samples showed ideal tetragonal structure but for x = 0.9 and 1.0 in the sintered of 1000°C, it was found that the tetragonality has disappeared. It is widely known that tetragonality is very much dependent on sintering temperature. To study the variation of tetragonality with sintering temperature the samples were sintered at 1100°C. At the sintering temperature of 1100°C the samples were again found to be of cubic spinel structure. At 1100°C, X-ray diffraction pattern reveals apparent transformation to cubic structure though some tetragonality may persist even at higher sintering temperature for higher copper content. It does not follow Vegard's law for higher concentration of x, because of structural change at higher Cu content and sintering temperature. X-ray and bulk densities are increased with increasing of Cu content. This can be ascribed to the atomic weight and density of Cu^{2+} (63.55, 8.94 g/cm^3, respectively) which are higher than that of Li^+ (6.94, 0.53 g/cm^3,) and Fe^{3+} (55.85, 7.87 g/ cm^3).

Sensitivity of electrical and magnetic properties depend on the microstructure of the ferrite sample. Permeability is directly proportional to the grain size. The average grain size was calculated by the linear intercept method. Grain size usually increases with the increasing of Cu content. Magnetization is defined as the magnetic moment per unit volume. Saturation magnetization has been measured in a Vibrating Sample Magnetometer (**VSM**) at room temperature. The decrease of A-B interaction was observed that the decreases of saturation magnetization with the increase of Cu^{2+} ions. Using the values of saturation magnetization, the experimental magnetic moment (in Bohr magneton) has been calculated for different compositions. Curie temperature is a measure of exchange force in ferrimagnetism. It is the temperature at which the thermal energy tends to disorder the system just to win over the exchange energy tending to order the system magnetically. At this temperature, ferrimagnetic substance change their phase over to a paramagnetic substance. For sintering temperature 1100°C, the values of Curie temperature for $Li_{0.5}Fe_{2.5}O_4$ and $CuFeO_4$ were found to be 675°C

and 425^{o}C, respectively. These values are in agreement with the literature values of T_C, which are 670^{o}C and 455^{o}C for Li ferrite and Cu ferrite. With the increase of Cu content, T_C decreases because both the magnetic moments μ_A and μ_B and also the net magnetic moment μ_m are reduced for the increase of x from x = 0 to 1. This behavior can be explained as follows: the substitution of the high spin quantum number Fe^{3+} (5) by the low spin quantum number Cu^{2+} (1) either at B-site or A-site, weakens the A-B interaction and causes a reduction in the molecular hyperfine field, H_m. This leads to a decrease in saturation magnetization and consequently a decrease in the Curie temperature T_C. It is concluded that T_C decreases more linearly with Cu content for the sintering of 1200^{o}C than the sintering of 1100^{o}C and nonlinearity at higher Cu content decreases with the increase of sintering temperature. It is due to the fact that structural change at higher Cu content for the higher sintering temperature. The initial permeability of $CuFe_2O_4$ is higher than other composition. This is because the sintered density is highest and the porosity is lowest for this composition. This shows that the high permeability ferrite can be used in high quality coils as a core. Coercivity and hysteresis loss decrease with the increase of Cu content due to increased magnetic softness at the Cu-rich end.

$Li_{0.5-x/2}Cu_xFe_{2.5-x/2}O_4$ have established that all the samples are n-type semiconductors. This indicates that the most probable conduction mechanism is electron hopping between Fe^{2+} and Fe^{3+} ions, $Fe^{2+} \bullet Fe^{3+} + e^{-}$ (n-type) At room temperature, the highest value of • is obtained for x = 0.3, but beyond this composition i.e. x > 0.3, resistivity decreases with increasing of Cu content, x. This indicate that Fe^{+2} ions are present as traces in the samples of x• 3. Activation energy increases with the increase of Cu content. The activation energy increases on changing from ferrimagnetic (E_f) to paramagnetic (E_p) region. The dielectric constant increases slowly with the temperature in the beginning and after that increases rapidly for different samples. The resistivity of ferrites decreases with increase in temperature. Thus by the electronic exchange $Fe^{2+} + Cu^{2+} \bullet Fe^{3+} + Cu^{+}$ one obtains local displacements of electrons in the direction of the applied field, these displacements determine the polarization of the ferrite. It is known that the effect of polarization is to reduce the field inside the medium. Hence, the dielectric constant is decreased as the frequency is increased.